Chamonium-Nucleon Scattering with Spin-Dependent Forces from Lattice QCD

Takuya Sugiura

February 4, 2019

Abstract

Since charmonium and nucleon do not have common valence quarks, color-singlet meson exchange forces are suppressed by the OZI rule. The $\eta_c N$ and the $J/\psi N$ interactions are thus dominated by the QCD van der Waals interaction. Although the QCD van der Waals interaction works to any hadron-hadron scattering, there is much less information of it compared to ordinary meson exchange interactions.

We study the $\eta_c N$ and the $J/\psi N$ interactions by lattice QCD first-principle calculations. For this purpose we employ the method developed by HAL QCD collaboration, where short-ranged spacial part of a hadron correlation function is utilized to define a potential faithful to the QCD S-matrix. We find that the $\eta_c N$ and the $J/\psi N$ (either with $J = 1/2$ or $J = 3/2$) interactions are all attractive. The qualitative behavior is similar in all cases, demonstrating expectation from the heavy quark symmetry. The $\eta_c N$ interaction is a little weaker than the $J/\psi N$ interaction. This result seems to be consistent with chromoelectric dipole picture of the QCD van der Waals interaction. Also, the $J/\psi N$ interaction depends weakly on the total angular momentum J. We derive the general form of the $J/\psi N$ interaction at the lowest order of the derivative expansion to find that it consists of the central, the spin-spin, and two types of tensor forces. The four forces are calculated in lattice QCD for the first time. The result shows that the spin-spin interaction strengthens the $J/\psi N$ attraction for $J = 1/2$, while it weakens the attraction for $J = 3/2$.

Contents

Chapter 1

Introduction

1.1 QCD and Effective Field Theories

The fundamental theory for the strong interaction is quantum chromodynamics (QCD). It, together with the Weinberg-Salam model for the electroweak interaction, constitutes the standard theory of elementary particles. As many as a few hundred species of hadrons listed in Particle Data Group [1] are composite states of quarks and gluons. All the hadrons belong to the singlet representation of the QCD electric charge, or *color*. This property of QCD is called the confinement, and is a consequence of the large gauge coupling constant in low-energy regime.

Since quarks are confined inside of the hadrons, it is useful to effective field theories with hadrons as elementary degrees of freedom [2]. The most important and well-understood example is the two-nucleon interactions [3, 4]. At large relative distance, the NN interaction is dominated by one-pion exchange. As the two nucleons come closer, exchange of heavier mesons (ρ, ω, and σ) and two-pion exchange become more significant. phenomenological potentials built upon the meson exchange picture have turned out to be successfully reproduce experimental NN scattering data with precision [5–7].

While a study of nuclear forces provides insight to the dynamics of light mesons which are produced by the spontaneous breaking of chiral symmetry, the interactions of heavy quarkonium, *i.e.*, a bound state of a heavy quark Q and an anti heavy quark $\bar{Q}$, have another importance. The essential difference between nucleon-nucleon interactions and quarkonium-nucleon interactions is that, in the latter case there is no common valence quarks. Thus, light meson exchange forces are suppressed by the OZI-rule [8–10] in the quarkonium-nucleon interactions. For the same reason, the Pauli exclusion principle does not apply at short distances. The dominant effects come from multi-gluon exchange forces, which is known as the QCD van der Waals interaction. Therefore, the heavy quarkonium-nucleon interactions are the best testing ground to study the QCD van der Waals interaction. Although the QCD van der Waals interaction works to any hadron-hadron scattering, there is much less information of it compared to ordinary meson exchange interactions. It is also related to non-perturbative properties of low-energy gluons.

Through analogy with the QED van der Waals interaction, the QCD van der Waals interaction is expected to be attractive [11–13]. Possible bound states of charmonium with nuclei are studied in Refs. [14–16]

1.2 Phenomenological Description of the Charmonium-Nucleon Interactions

A heavy quarkonium $Q\bar{Q}$ is spatially small, as the scale of its radius is set by the inverse quark mass. Appelquist, Dine, and Muzinich [17] have argued that its interaction with gluons is also localized in time if the radius of the quarkonium is sufficiently small that the interaction between Q and $\bar{Q}$ is dominated by the one-gluon exchange, *i.e.*, it is a Coulomb bound state. Therefore, gluons emitted from a sufficiently heavy quarkonium must assemble into color-singlet clusters which is localized both in space and time. The use of an operator product expansion [18–21] is justified in this context, as discussed by Peskin [22]. It turns out to be theoretically equivalent to a multipole expansion [23,24]. Luke, Manohar, and Savage [11] have applied the idea to an effective Lagrangian.

The operators of the lowest dimension are the square of the chromoelectric field $(\boldsymbol{E}^a)^2$ and the square of the chromomagnetic field $(\boldsymbol{B}^a)^2$. The latter is much smaller than the former, since the strength of the magnetic field is smaller by a factor of $\alpha_s(\Lambda_Q)$ than the electric field, where $\Lambda_Q = r_Q^{-1} = \alpha_s(r_Q^{-1})m_Q$ is the inverse quarkonium radius. Therefore, the amplitude for the scattering of a heavy quarkonium with another hadron h can be written in the heavy quark limit as [1]

$$\mathcal{M} = \frac{1}{3}g^2 \left\langle \Phi' \left| r^i \frac{1}{\epsilon + H_a} r^j \right| \Phi \right\rangle \left\langle h' \left| \frac{1}{2} E_i^a E_j^a(0) \right| h \right\rangle , \tag{1.1}$$

where $|\Phi\rangle$ and $|h\rangle$ are the QCD eigenstates of a single quarkonium and a single h, respectively; $\boldsymbol{r}$ is the relative coordinate of Q and $\bar{Q}$; H_a is the non-relativistic Hamiltonian for the internal motion of the $Q\bar{Q}$ system in a color octet state; ϵ is the binding energy of $Q\bar{Q}$. The gauge coupling g is evaluated at the scale Λ_Q. By defining the chromoelectric polarizability α^{ij} as

$$\alpha^{ij} \equiv \frac{1}{3} \left\langle \Phi' \left| r^i \frac{1}{\epsilon + H_a} r^j \right| \Phi \right\rangle , \tag{1.2}$$

Eq. (1.1) can be written as

$$\mathcal{M} = \frac{g^2}{2} \alpha^{ij} \left\langle h' \left| E_i^a E_j^a(0) \right| h \right\rangle . \tag{1.3}$$

The chromoelectric polarizability is solely determined by the quarkonium properties, while the matrix element $\langle h' \,|\, E_i E_j \,|\, h \rangle$ is solely from the light-degrees of freedom, *i.e.*, the light quarks

[1] The relativistically normalized scattering amplitude is $\mathcal{M}_{\rm rel} = (2\pi)^4 \delta^4(\sum \boldsymbol{p})(2m_{Q\bar{Q}})\mathcal{M}$.

and soft gluons. If the quarkonium has S-wave orbital angular momentum, it does not depend on the angle i and j, so that $\alpha^{ij} = \delta^{ij}\bar{\alpha}$. Equation (1.2) can be analytically computed as one expands it in $1/N_c$, where N_c is the number of colors. At $\mathcal{O}(1/N_c^0)$, α for the 1S and 2S Coulombic quarkonium states are given as

$$\alpha^{ij}(1\mathrm{S} \to 1\mathrm{S}) = \delta^{ij}\frac{4}{27}\pi a_0^3 \cdot 7, \tag{1.4}$$

$$\alpha^{ij}(2\mathrm{S} \to 2\mathrm{S}) = \delta^{ij}\frac{4}{27}\pi a_0^3 \cdot 502, \tag{1.5}$$

where $a_0 = (16\pi)/(3g^2 m_Q)$ is the Bohr radius of the quarkonium. One may apply the above discussion to the charmonium state, although the charm quark might not be heavy enough to form a Coulombic $c\bar{c}$ bound state. Then the S-wave charmonium chromoelectric polarizabilities are calculated as [25, 26]

$$\bar{\alpha}(1\mathrm{S} \to 1\mathrm{S}) \simeq 0.2\,\mathrm{GeV}^{-3}, \tag{1.6}$$

$$\bar{\alpha}(2\mathrm{S} \to 2\mathrm{S}) \simeq 12\,\mathrm{GeV}^{-3}, \tag{1.7}$$

$$\bar{\alpha}(2\mathrm{S} \to 1\mathrm{S}) \simeq -0.6\,\mathrm{GeV}^{-3}. \tag{1.8}$$

Meanwhile, a phenomenological evaluation of the transition polarizability $\bar{\alpha}(2\mathrm{S} \to 1\mathrm{S})$ from the decay $\psi' \to J/\psi\pi\pi$ gives [27]

$$|\bar{\alpha}(2\mathrm{S} \to 1\mathrm{S})| \simeq 2\,\mathrm{GeV}^{-3}. \tag{1.9}$$

No other result has been reported phenomenologically for the charmonium chromoelectric polarizabilities. Recently, Polyakov and Schweitzer [29] have utilized our preliminary lattice result of the $J/\psi N$ interactions [28] to determine the 1S diagonal element as

$$\bar{\alpha}(1\mathrm{S} \to 1\mathrm{S}) = 1.5 \pm 0.6\,\mathrm{GeV}^{-3}, \tag{1.10}$$

with unphysical quark masses, $m_\pi = 874\,\mathrm{MeV}$ and $m_N = 1816\,\mathrm{MeV}$. All the above values roughly agree, but with large uncertainties. More detailed analysis is required to determine α with more precision. Also, it is very important to check to what extent the chromoelectric dipole picture works for charmonium-nucleon interactions. Especially, the 2S state has relatively large size than the 1S state, so that the assumption of Coulombic bound state is questionable for the 2S.

The chromoelectric dipole interaction in Eq. (1.1) appears at the lowest order of the multipole expansion; higher-order terms can also be systematically considered. For example, the spin-spin interaction between a J/ψ and a nucleon arises due to interference of the chromoelectric dipole and the chromomagnetic quadrupole transitions [25]. This the next-to-leading order effect, *i.e.*, suppressed by a factor of $\mathcal{O}(1/m_c)$ relative to the leading spin-independent interaction.

Chapter 2

Inverse Scattering in a Finite Box

2.1 Non-Relativistic Scattering

We consider a non-relativistic scattering problem of two spinless particles in 3-dimensional space. The Hamiltonian in the center of mass frame is written as

$$H = -\frac{\boldsymbol{\nabla}^2}{2\mu} + V(r) \qquad r = |\boldsymbol{r}|\,, \tag{2.1}$$

where $\boldsymbol{r}$ is the relative coordinate of the two particles and μ is the reduced mass. The interaction is assumed to be local, smooth and short-ranged, such that there exists a range R and $V(r) = 0$ for $r > R$. The wave function is a solution to the stationary Schrödinger equation

$$H\psi(\boldsymbol{r}) = E\psi(\boldsymbol{r}), \tag{2.2}$$

where E is the energy eigenvalue. By separating the wave function as

$$\psi(\vec{r}) = \sum_{l=0}^{\infty} \sum_{m=-l}^{+l} \frac{\phi_l(r)}{r} Y_{lm}(\theta, \varphi), \tag{2.3}$$

$$\boldsymbol{r} = (r\sin\theta\cos\varphi,\ r\sin\theta\sin\varphi,\ r\cos\theta)\,, \tag{2.4}$$

eq. (2.2) splits into the angular equation

$$\left[\frac{1}{\sin\theta}\frac{\partial}{\partial\theta}\left(\sin\theta\frac{\partial}{\partial\theta}\right) + \frac{1}{\sin^2\theta}\frac{\partial^2}{\partial\varphi^2}\right] Y_{lm}(\theta,\varphi) = l(l+1)Y_{lm}(\theta,\varphi), \tag{2.5}$$

and the radial Schrödinger equation

$$\left[\frac{\partial^2}{\partial r^2} - \frac{l(l+1)}{r^2} + k^2 - 2\mu V(r)\right]\phi_l(r) = 0, \tag{2.6}$$

where the momentum k is related to the energy E through $E = k^2/(2\mu)$. The functions $Y_{lm}(\theta,\varphi)$ are well-known as the spherical harmonics, and our main interest is on the radial

wave function $\phi_l(r)$. We here focus on scattering states, *i.e.* $E > 0$ and k is real. Note that, for large enough l, the centrifugal barrier $l(l+1)/r^2$ prevents the two particle to be within the range of the potential $r < R$ and "feel each other" to be scattered. *The partial wave expansion* (2.3) can be truncated for l at some $l = l_{\max}$, since $l > l_{\max}$ would give a trivial result and are none of our interest. One would find $l_{\max}$ smaller for smaller k^2, since if the relative momentum is small it is unlikely that the particles penetrate the centrifugal barrier; this is why the partial wave expansion is especially useful for low-energy scattering.

Let us first consider the free case when $V(r) = 0$ for all $r \in \mathbb{R}$. As $r \to 0$, the centrifugal term $l(l+1)/r^2$ dominates over the energy term k^2, and thus $\phi_l(r)$ must behave like either r^{l+1} or r^{-l}. The two independent solutions are known as the Riccati-Bessel function $\hat{j}_l(kr)$ and the Riccati-Neumann function $\hat{n}_l(kr)$, respectively,

$$\hat{j}_l(z) \equiv z j_l(z) = \left(\frac{\pi z}{2}\right)^{1/2} J_{l+1/2}(z), \tag{2.7}$$

$$\hat{n}_l(z) \equiv z n_l(z) = (-1)^l \left(\frac{\pi z}{2}\right)^{1/2} J_{-l-1/2}(z), \tag{2.8}$$

where $j_z(z)$ is the spherical Bessel function, $n_l(z)$ is the spherical Neumann function, and $J_\lambda(z)$ is the ordinary Bessel function satisfying

$$\left(z^2 \frac{d^2}{dz^2} + z\frac{d}{dz} + (z^2 - \lambda^2)\right) J_\lambda(z) = 0. \tag{2.9}$$

In the free case, the physically relevant solution is given by $\hat{j}_l(kr)$, as it vanishes at $r = 0$ and $\hat{n}_l$ does not. As $r \to \infty$, the centrifugal force vanishes and the $\phi_l(r)$ behaves like the solutions of $l = 0$. For this it is more convenient to introduce the Riccati-Hankel functions

$$\hat{h}_l^{(\pm)}(z) \equiv \hat{n}_l(z) \pm i\hat{j}_l(z), \tag{2.10}$$

which has the asymptotic form

$$\hat{h}_l^{(\pm)}(z) \underset{z\to\infty}{\to} \exp\left(\pm i(z - l\pi/2)\right). \tag{2.11}$$

From the above definitions it is clear that for $x \in \mathbb{R}$, $\hat{j}_l(x)$ and $\hat{n}_l(x)$ are real, and

$$\left[\hat{h}_l^{(\pm)}\right]^* = \hat{h}_l^{(\mp)}. \tag{2.12}$$

For finite $V(r)$, the following boundary condition is introduced at $r = 0$:

$$\lim_{r\to 0}\left(\phi_l(r)/\hat{j}_l(kr)\right) = 1, \tag{2.13}$$

that is, $\phi_l(r)$ behaves as r^{l+1} with normalization defined by the Riccati-Bessel function. In the limit $r \to \infty$ (or in our present model for $r > R$), the potential vanishes and $\phi_l(r)$ is expressed as a linear combination of the the Riccati-Hankel functions:

$$\phi_l(r) = \frac{i}{2}\left(F_l(k)\hat{h}_l^{(-)}(kr) - F_l^*(k)\hat{h}_l^{(+)}(kr)\right). \tag{2.14}$$

Since both the boundary condition (2.13) and the radial Schrödinger Eq. (2.6) contain real quantities only, $\phi_l(r)$ is real; this is reflected to the fact that the coefficients are given by a complex-valued function $F_l(k)$ and its complex conjugate. The function $F_l(k)$ is called the Jost function, and is related to the S-matrix element through

$$s_l(k) = \frac{F_l^*(k)}{F_l(k)}. \tag{2.15}$$

From this expression it is clear that $s_l(k)$ has modulus unity and thus it is parameterized by a real quantity $\delta_l(k)$ called the phase shift, as

$$s_l(k) = \exp\left(2i\delta_l(k)\right). \tag{2.16}$$

By definition, the phase shift has ambiguity of modulus π. Usually, the ambiguity is removed by requiring that $\delta_l(k)$ be a continuous function of k that goes to zero as $k \to \infty$: if the energy is so large that $k^2 \gg V(r)$ for all r, there occurs hardly any scattering. With the above definition, the phase shift at $k = 0$ is related to the number of bound states n_l with the given l:

$$\delta_l(0) = n_l\pi, \tag{2.17}$$

unless $F_0(0) = 0$, in which case the same result holds for $l > 0$ but $\delta_0(0) = (n_0 + 1/2)\pi$. It is known that the sign of the potential and the sign of the phase shift are related. In particular, a wholly attractive potential ($V(r) < 0$ for all r) gives a positive phase shift, while a wholly repulsive potential gives a negative phase shift.

We note that the solution satisfying Eq. (2.14) is called *the regular solution*. Another commonly used solution which we denote as $\psi_l(r)$ satisfies

$$\psi_l(r) = \hat{j}_l(kr) + kf_l(k)\hat{h}_l^{(+)}(kr) \tag{2.18}$$

for $r > R$, where *the partial wave amplitude* $f_l(k)$ is defined as

$$f_l(k) = \frac{s_l(k) - 1}{2ik}. \tag{2.19}$$

The two solutions are related through

$$\phi_l(r) = F_l(k)\psi_l(r). \tag{2.20}$$

The advantage of working with the regular solution $\phi_l(r)$ lies in the fact the boundary condition is given at $r = 0$ only and thus it is mathematicaly more convenient. Especially, when we convert the differential radial Schrödinger Eq. (2.6) to an integral equation, we can solve it point-by-point for each r from the origin.

2.2 Quantum Mechanics in Finite Volume

We now place the two particles in a finite box of size L^3 with periodic boundary conditions. The stationary Schrödinger equation becomes

$$\left(-\frac{\boldsymbol{\nabla}^2}{2\mu} + V_L(r)\right)\psi_n(\boldsymbol{r}) = E_n\psi_n(\boldsymbol{r}), \tag{2.21}$$

where the potential is defined through the potential in the infinite volume $V(r)$ as

$$V_L(r) = \sum_{\boldsymbol{n}\in\mathbb{Z}^3} V(|\boldsymbol{r}+L\boldsymbol{n}|), \tag{2.22}$$

to take into account the interactions "around the world". The wave function $\psi_n(r)$ satisfies

$$\psi_n(\boldsymbol{r}+L\boldsymbol{n}) = \psi_n(\boldsymbol{r}), \qquad \boldsymbol{n}\in\mathbb{Z}^3, \tag{2.23}$$

which can be made orthonormal to form a complete set of smooth eigenfunctions. Unlike in the infinite volume case, the energy eigenvalues $E_n = k_n^2/(2\mu)$ are discretized in a finite volume. The larger the box size is, the more states are allowed to exist. As $L\to\infty$, the spectrum becomes infinitely dense in the positive energy region to be the continuous scattering states, while the bound states remain discrete in the negative energy region. It is important to remember that negative $E_n(L)$ for a given finite L does not necessarily imply the existence of a bound state in the limit $L\to\infty$.

In a finite box we cannot separate the two particles infinitely apart, unlike in the infinite volume case. However, if the box size is sufficiently larger than the potential range such that $L > 2R$, we can define the "exterior region" $\Omega_{\rm ex}$ and the "inner region" $\Omega_{\rm in}$ by

$$\Omega_{\rm ex} = \left\{\boldsymbol{r}\in\mathbb{R}^3 \mid |\boldsymbol{r}+\boldsymbol{n}L| > R, \boldsymbol{n}\in\mathbb{Z}^3\right\}, \tag{2.24}$$

$$\Omega_{\rm in} = \left\{\boldsymbol{r}\in\mathbb{R}^3 \mid |\boldsymbol{r}+\boldsymbol{n}L| < R, \boldsymbol{n}\in\mathbb{Z}^3\right\}. \tag{2.25}$$

In the exterior region, the potential vanishes and $\psi_n(\boldsymbol{r})$ satisfies the Helmholtz equation

$$\left(\boldsymbol{\nabla}^2 + k_n^2\right)\psi_n(\boldsymbol{r}) = 0, \tag{2.26}$$

with the boundary condition (2.23). In a finite volume, the rotational symmetry is reduced to its subgroup. Representations in the finite volume are expressed by a linear combination of a few states with different angular momentum.

Now, since k_n are restricted to those which are accommodated in the box with periodicity, we can relate the discretized spectrum to the phase shift. The relation has been rigorously studied by M. Lüscher [30–32], and thus is called *Lüscher's finite volume formula*. We give a brief introduction to this formula in Sec. 2.3. Another possible strategy is to find a quantity which can be calculated by lattice QCD and has the asymptotic form (2.14) up to small corrections due to finite L. Then the potential is defined to satisfy Schrödinger Eq. (2.21) for given energies and the corresponding "wave functions". The latter method is developed by the HAL QCD collaboration, and is the topic of Sec. 2.4. It is important to note that the two methods are theoretically equivalent, although they look somewhat different at first sight.

2.3 Luscher's Finite Volume Method

In Refs. [30, 31], Lüscher has considered the volume dependence of the discretized energy spectrum. He has found that the finite volume energy shift due to the polarization effects decreases exponentially with L, whereas the physically relevant, interaction in the range $r < R$ gives rise to corrections of powers of L. This observation can be intuitively understood as follows: since the wave functions are spread throughout the box, the probability of finding two particles within $r < R$ is inversely proportional to the volume. Further detailed analysis gives the following expansion of the lowest-lying energy level E_0 in a power series of $1/L$:

$$E_0 = -\frac{2\pi a_0}{\mu L^3}\left\{1 + c_1\frac{a_0}{L} + c_2\frac{a_0^2}{L^2}\right\} + \mathcal{O}(L^{-6}), \tag{2.27}$$

$$c_1 = -2.837297, \tag{2.28}$$

$$c_2 = 6.375183, \tag{2.29}$$

where a_0 is defined through the effective range expansion

$$k\cot\delta_0(k) = -\frac{1}{a_0} + \frac{r_0}{2}k^2 + \mathcal{O}(k^4). \tag{2.30}$$

The S-wave scattering length a_0, together with the effective range r_0, gives one of the most important parameterization for low-energy scattering. Expansion (2.27) is valid to all orders of perturbation. It is clear from this expression that the energy eigenvalue in a finite box has simple relation to the S-matrix elements.

Although Eq. (2.27) is a very important result, it is practically desirable to find a simpler relation of the energy spectrum to the phase shift. We first note that this issue is extremely simple on a $1+1$ dimensional space-time. Since the free wave in this case is either $e^{-ik|x|}$ or $e^{+ik|x|}$, a parity-even solution outside in the exterior region is given by

$$\psi_n(x) = e^{-ik_n|x|} + e^{2i\delta_0(k_n)}e^{ik_n|x|}, \tag{2.31}$$

where the irrelevant overall normalization factor is omitted. Requiring the wave function to satisfy periodicity

$$\left.\frac{d}{dx}\psi_n(x)\right|_{r=L/2} = 0, \tag{2.32}$$

one finds

$$e^{2i\delta_0(k_n)} = e^{-ik_nL}. \tag{2.33}$$

Thus once the discretized spectrum $E_n = k^2/(2\mu)$ is obtained, the phase shift can be calculated as $\delta_0(k_n) = m\pi - \frac{1}{2}k_nL$, with $m \in \mathbb{Z}$ fixed by the condition (2.17).

In $1+3$ dimensions, the situation is much more complicated, since the 3-dimensional rotational symmetry SO(3) is explicitly broken to its subgroup O with respect to rotation of

unit $\pi/2$. Therefore, the partial wave expansion does not give a basis of the eigenfunctions, preventing simple arguments of the above kind. Lüscher [32] has rigorously studied the properties of the Helmholtz equation on a 3-dimensional torus to finally find the corresponding analogue of Eq. (2.33). In particular, the S-wave scattering states of two scalar particles in the infinite volume corresponds to the A_1^+ representation of the cubic group. Neglecting small contributions from $l \geq 4$, S-wave phase shift can be calculated through

$$k_n \cot \delta(k_n) = \frac{1}{\pi L} \sum_{\boldsymbol{n} \in \mathbb{Z}^3} \frac{1}{\boldsymbol{n}^2 - (k_n L/2\pi)^2}. \tag{2.34}$$

As it is apparent in this expression, Lüscher's finite volume method utilizes the fact that any scattering state in the exterior region has a unique matching free-wave solution with momentum $k = 2\pi |\boldsymbol{n}| / L$. In this sense it is instructive to say that the phase shift is calculated from the wave function in the exterior region.

2.4 HAL QCD Method

2.4.1 Time-Independent Method

Let us now consider a field theory that corresponds to the non-relativistic quantum mechanics defined by Eq. (2.1). The lagrangian is given by

$$L = L_0 + L_{\text{int}}, \tag{2.35}$$

$$L_0 = \int d^3\boldsymbol{x}\, \phi^\dagger(x) \left(i\partial_\tau + \frac{\boldsymbol{\nabla}^2}{2m} \right) \phi(x), \tag{2.36}$$

$$L_{\text{int}} = \frac{1}{2} \int d^3\boldsymbol{x} d^3\boldsymbol{y}\, \phi^\dagger(x)\phi^\dagger(y)\, V(|\boldsymbol{x} - \boldsymbol{y}|)\, \phi(x)\phi(y), \tag{2.37}$$

where $\phi(x)$ is a scalar field and with mass $m = 2\mu$ and 4-vectors in the Minkowsi space are represented as $x = x_\nu = (\boldsymbol{x}, \tau)$. The canonical momentum field $\pi(x)$ is defined through $S = \int dt L$ as

$$\pi(x) = \frac{\delta S}{\delta \dot{\phi}(x)} = i\phi^\dagger(x). \tag{2.38}$$

The Hamiltonian is then

$$H = \int d^3\boldsymbol{x}\, \pi(x)\dot{\phi}(x) - L \tag{2.39}$$

$$= -i \int d^3\boldsymbol{x}\, \pi(x) \left(-\frac{\boldsymbol{\nabla}^2}{2m} \right) \phi(x) + L_{\text{int}}. \tag{2.40}$$

To quantize the field, we impose the equal-time canonical commutation relation

$$[\phi(\boldsymbol{x}, \tau), \pi(\boldsymbol{y}, \tau)] = i\delta^3(\boldsymbol{x} - \boldsymbol{y}), \tag{2.41}$$

or, equivalently,

$$\left[\phi(\boldsymbol{x},\tau),\phi^\dagger(\boldsymbol{y},\tau)\right]=\delta^3(\boldsymbol{x}-\boldsymbol{y}). \tag{2.42}$$

Given the above Hamiltonian, we can now define a quantity of crucial importance in our study. It is defined through

$$\langle 0\,|\,\phi(\boldsymbol{x},\tau)\phi(\boldsymbol{y},\tau)\,|\,E\rangle=\psi(\boldsymbol{x}-\boldsymbol{y})e^{-iE\tau}, \tag{2.43}$$

where $|E\rangle$ is the eigenstate of H with eigenvalue E:

$$H\,|E\rangle=E\,|E\rangle\,. \tag{2.44}$$

The vacuum $|0\rangle$ is defined as the zero-energy eigenstate, *i.e.* $H\,|0\rangle=0$, which implies

$$\phi(x)\,|0\rangle=0. \tag{2.45}$$

The function $\psi(\boldsymbol{x}-\boldsymbol{y})$ thus defined is called the *equal-time Nambu-Bethe-Salpeter (NBS) wave function*. This is a perfect analogue of the wave function in quantum mechanics, as it satisfies the stationary Schrödinger equation

$$\left(-\frac{\boldsymbol{\nabla}^2}{2\mu}+V(r)\right)\psi(\boldsymbol{r})=E\psi(\boldsymbol{r}). \tag{2.46}$$

It is quite easy to show Eq. (2.46) from the identity

$$\langle 0\,|\,[\phi(\boldsymbol{x},\tau)\phi(\boldsymbol{y},\tau),H]\,|\,E\rangle=E\psi(\boldsymbol{x}-\boldsymbol{y})e^{-iE\tau}. \tag{2.47}$$

Our non-relativistic field theory is purposefully designed to reproduce the Schrödinger equation. However, it implies that the NBS wave function can be utilized to study low-energy scattering in more realistic models. In fact, it has been shown that NBS wave functions in QCD has the asymptotic form of Eq. (2.14) up to normalization constants, solely from the properties of quantum field theories [33–35]. Therefore NBS wave functions in the exterior region contains information about the S-matrix, whereas its behavior in the inner region depends on the calculation scheme. To be specific, the $J/\psi N$ NBS wave function is defined by

$$\psi_{\alpha\mu}(\boldsymbol{x}-\boldsymbol{y})e^{-Wt}=\langle 0\,|\,N_\alpha(\boldsymbol{x},t)\psi_\mu(\boldsymbol{y},t)\,|\,W\rangle\,, \tag{2.48}$$

where $|W\rangle$ is the QCD eigenstate with total energy W and the quantum numbers of the $J/\psi N$ system, $N_\alpha(x)$ and $\psi_\mu(y)$ are local field operators of nucleon and J/ψ, respectively, and we have moved to the Euclidean space of imaginary time $t=i\tau$. The choice of interpolating operators is not unique: there are infinitely many degrees of freedom to combine quark operators into a local operator with the quantum numbers of these hadrons. This suggests that the structure of the NBS wave function is dependent on the choice of the interpolating operators. The important point is that the large-distance asymptotic behavior of the NBS wave function does not depend on the choice of the interpolating operators: the QCD S-matrix is unique. Further

discussion on the $J/\psi N$ NBS wave function will be given in the next chapter. Here let us continue our discussion with the scalar particles.

Suppose we know NBS wave functions $\psi_n(\boldsymbol{r})$ and associated energies $E_n = k_n^2/(2\mu)$ for $n \leq n_c$ from a field theory in a finite box. In this case, we "define" the potential through the Schrödinger equation

$$\left(\frac{\boldsymbol{\nabla}^2}{2\mu} + E_n\right)\psi_n(\boldsymbol{r}) = \int d^3\boldsymbol{r}'\, U(\boldsymbol{r},\boldsymbol{r}')\psi_n(\boldsymbol{r}'), \tag{2.49}$$

where we introduce an energy-independent and non-local potential $U(\boldsymbol{r},\boldsymbol{r}')$. It is crucial in the HAL QCD method that the potential be non-local: the principal quantities here are the NBS wave functions for given energies, and an energy-independent and local potential

$$U(\boldsymbol{r},\boldsymbol{r}') = \delta^3(\boldsymbol{r}-\boldsymbol{r}')V(\boldsymbol{r}) \tag{2.50}$$

cannot always satisfy Eq. (2.49) for all $n \leq n_c$ simultaneously [1]. This is in contrast to many other cases, where potentials are constrained to be local in the coordinate space. These local potential may be related to the non-local potential in Eq. (2.49) through the unitary transformation

$$\psi_n \to \psi' = A\psi, \tag{2.51}$$

$$U \to U' = AUA^\dagger \qquad A : \text{unitary matrix.} \tag{2.52}$$

Such unitary transformation changes the structure of the potential and the wave functions, but does not affect the observables of the theory, such as the energy eigenvalues and S-matrix elements. The potential defined by Eq. (2.49) is one of these potentials which reproduces the NBS wave functions in a box. In Ref. [34], it is shown that such an energy-independent and non-local potential actually exists.

In practice, the nonlocality of the HAL QCD potential is taken into account by the derivative expansion: the potential is expressed as a power series of spatial derivatives, coefficients of which are energy-independent and local functions. In our non-relativistic model of scalar particles with Hermiticity, rotational invariance, time-reversal invariance and parity symmetry, the potential is assumed to have the form

$$U(\boldsymbol{r},\boldsymbol{r}') = V(\boldsymbol{r},\boldsymbol{\nabla})\delta^3(\boldsymbol{r}-\boldsymbol{r}'), \tag{2.53}$$

$$V(\boldsymbol{r},\boldsymbol{\nabla}) = V_0(r) + \frac{1}{2}\left\{V_{v^2}(r),\boldsymbol{v}^2\right\} + V_{l^2}(r)\boldsymbol{l}^2 + \mathcal{O}(\boldsymbol{v}^4), \tag{2.54}$$

with $\boldsymbol{p} = -i\boldsymbol{\nabla}$, $\boldsymbol{v} = \boldsymbol{p}/\mu$, and $\boldsymbol{l} = \boldsymbol{r}\times\boldsymbol{p}$. The anticommutation relation in the second term of the right-hand side is necessary to require the potential to be Hermite. The higher-order terms involve spatial derivatives, and they correspond to the relative momentum of the

[1] There is a possibility that a local potential satisfy the Schrödinger equation at several different energies by chance; however this is unlikely since we do not intend it. The derivative expansion is introduced with expectation that at low energies a local potential approximates the non-local potential in Eq. (2.49), but the applicability of the local approximation must be checked in every case.

two particles. Therefore the series is expected to converge in a sense that the low-energy scattering is well described by first a few terms. In Ref. [36], we have numerically confirmed the convergence of the derivative expansion with a similar model in 1+1 dimensions. If we neglect the terms of $\mathcal{O}(\boldsymbol{v}^4)$, there are five linearly-independent functions in Eq. (2.54): V_0, V_{v^2}, $(\partial/\partial r)V_{v^2}$, $(\partial^2/\partial r^2)V_{v^2}$, and V_{l^2}. If we have five linearly independent wave functions for energies $E_0, \cdots, E_4$, we can solve Eq. (2.49) for these functions.

In the HAL QCD method, the potential is calculated from the wave functions in the inner region. In the outer region, the potential vanishes since the wave functions satisfy the Helmholtz equation and the left-hand side of Eq. (2.49) becomes zero. The finite-volume effect in the inner region is exponentially suppressed, making extrapolation to $L \to \infty$ an easy task: we fit the resulting potential by functions that goes to zero as $r \to \infty$ fast enough, and then solve the Schrödinger equation in a infinite volume. When studying the bound states, this is an important advantage of the HAL QCD method over Lüscher's finite volume method, where the periodic boundary condition plays an essential role and thus the limit $L \to \infty$ needs to be taken with much more care.

2.4.2 Time-Dependent Method

In lattice QCD, the equal-time NBS wave function cannot be directly calculated; instead, we get a mixture of states with different energies,

$$C(\boldsymbol{r}, t) = \sum_n A^n \psi_n(\boldsymbol{r}) e^{-W_n t}, \tag{2.55}$$

where n labels the QCD eigenstates with momentum $k_n = |\boldsymbol{k}_n|$,

$$W_n = \sqrt{k_n^2 + m_1^2} + \sqrt{k_n^2 + m_2^2}, \tag{2.56}$$

$$\frac{1}{\mu} = \frac{1}{m_1} + \frac{1}{m_2}, \tag{2.57}$$

and A_n are unknown coefficients. To calculate the potential from Eq. (2.49), we need to extract each wave functions from here. In the Euclidean space, the imaginary-time t appears in the exponents with a factor $-W_n$. For sufficiently large t, excited-state contributions to Eq. (2.55) are suppressed, such that

$$C(\boldsymbol{r}, t) \sim A^0 \psi_0(\boldsymbol{r}) e^{-W_0 t}, \qquad t \gg 1/(W_1 - W_0). \tag{2.58}$$

This condition is called the ground-state saturation. When the ground-state saturation is achieved, the NBS wave function for $n = 0$ equals to Eq. (2.55) upto the irrelevant normalization factor.

However, the above procedure is hard to follow in actual situations because the signal-to-noise ratio in the correlation function (2.55) becomes exponentially small for large t. Therefore, as we go to large t region to achieve the ground-state saturation, the signal of the correlation

function gets weaker. Moreover, the splitting $W_1 - W_0$ becomes smaller as $1/L^2$: for example, in the free case, it is assumed as

$$W_1 - W_0 = \frac{1}{2\mu}\frac{(2\pi)^2}{L^2}. \tag{2.59}$$

This means that, to achieve the ground-state saturation in a very large box, the imaginary time t needs to be very large, where statistical noise is terrible. We need a better method to calculate potentials by lattice QCD.

In Ref. [37], the above problem is avoided by utilizing the imaginary-time dependence of the correlation function. One defines a normalized correlation function

$$R(\boldsymbol{r}, t) = C(\boldsymbol{r}, t) \times e^{(m_1+m_2)t} \tag{2.60}$$

$$= \sum_n A^n \psi_n(\boldsymbol{r}) e^{-\Delta W_n t}, \tag{2.61}$$

with $\Delta W = W_n - (m_1 + m_2)$. If the two particles are identical, *i.e.*, $m_1 = m_2 = 2\mu$, one finds the identity

$$\frac{k_n^2}{2\mu} = \Delta W_n + \frac{\Delta W_n^2}{8\mu}, \qquad \text{if } m_1 = m_2. \tag{2.62}$$

If $m_1 \neq m_2$, one expands ΔW_n in powers of k_n to find

$$\frac{k_n^2}{2\mu} = \Delta W_n + \frac{1+3\delta^2}{8\mu}\Delta W_n^2 + \delta^2 \cdot \mathcal{O}(k_n^6), \tag{2.63}$$

$$\delta = \frac{m_1 - m_2}{m_1 + m_2}. \tag{2.64}$$

As far as we are interested in low-energy scattering, the terms of $\mathcal{O}(k_n^6)$ are supposed to be small and can be safely neglected. Then Eq. (2.63) implies that the kinetic energy $E_n = k_n^2/(2\mu)$ can be extracted from the normalized correlator (2.60) by temporal derivatives:

$$\left(\frac{1+3\delta^2}{8\mu}\frac{\partial^2}{\partial t^2} + \frac{\partial}{\partial t}\right) R(\boldsymbol{r}, t) = \sum_n \frac{k_n^2}{2\mu} A^n \psi_n(\boldsymbol{r}) e^{-\Delta W_n t} \tag{2.65}$$

$$= \sum_n A^n \left(-\frac{\boldsymbol{\nabla}^2}{2\mu}\psi_n(\boldsymbol{r}) + \int d^3\boldsymbol{r}'\, U(\boldsymbol{r}, \boldsymbol{r}')\psi_n(\boldsymbol{r}')\right) e^{-\Delta W_n t}, \tag{2.66}$$

where we have used Eq. (2.43) to obtain the last equation. Recall that the HAL QCD potential is defined by Eq. (2.43) with given $E_n = k_n^2/(2\mu)$ and $\psi_n(\boldsymbol{r})$ for $n \leq n_c$: all the elastic states below the meson production threshold are reproduce by the same potential. It is now clear that the same potential $U(\boldsymbol{r}, \boldsymbol{r}')$ satisfy the following time-dependent Schrödinger-like equation:

$$\left(\frac{1+3\delta^2}{8\mu}\frac{\partial^2}{\partial t^2} + \frac{\partial}{\partial t} + H_0\right) R(\boldsymbol{r}, t) = \int d^3\boldsymbol{r}'\, U(\boldsymbol{r}, \boldsymbol{r}') R(\boldsymbol{r}', t), \tag{2.67}$$

where $H_0 = \boldsymbol{\nabla}^2/(2\mu)$. The method which uses Eq. (2.67) to calculate the potential is called the "time-dependent HAL QCD method" hereafter. The principal advantage of the time-dependent HAL QCD method over the previous, time-independent method is that we do not have to separate each wave function from the correlator (2.55). In Eq. (2.67), the fact that all the wave functions are reproduced by a single energy-independent and non-local potential is more explicitly utilized. As a result, what we require is not the ground-state saturation, but the elastic-state saturation

$$C(\boldsymbol{r}, t) \sim \sum_{n=0}^{n_c} A^n \psi_n(\boldsymbol{r}) e^{-W_n t}, \tag{2.68}$$

where n_c is set by the meson production threshold. Such t required for the elastic-state saturation is in general much smaller than what is required for the ground-state saturation, allowing us to obtain good signals in lattice QCD simulations.

Once the elastic-state saturation is achieved, we can apply the derivative expansion to the non-local potential as in Eqs. (2.53) and (2.54). If we take the lowest order (central force) of the expansion, *i.e.*, $U(\boldsymbol{r}, \boldsymbol{r}') = V_0(r)\delta^3(\boldsymbol{r} - \boldsymbol{r}')$, we get

$$\left(\frac{1 + 3\delta^2}{8\mu} \frac{\partial^2}{\partial t^2} + \frac{\partial}{\partial t} + H_0 \right) R(\boldsymbol{r}, t) = V_0(r) R(\boldsymbol{r}, t). \tag{2.69}$$

The convergence of the derivative expansion can be confirmed by seeing the t-independence of the central potential $V_0(r)$ thus determined.

Chapter 3

Charmonium-Nucleon Interactions

3.1 Charmonium-Nucleon Wave Functions

3.1.1 Nambu-Bethe-Salpeter Wave Function

The $J/\psi N$ NBS wave function is extracted from the correlation function

$$C_{\alpha\mu;\alpha'\mu'}(\boldsymbol{r}, t-t_0) = \sum_{\boldsymbol{x}} \left\langle 0 \left| N_\alpha(\boldsymbol{r}+\boldsymbol{x}, t)\psi_\mu(\boldsymbol{x}, t)\bar{\mathcal{J}}^{(J^P)\mathrm{wall}}_{\alpha'\mu'}(t_0) \right| 0 \right\rangle, \tag{3.1}$$

where $N_\alpha(x)$ and $\psi_\mu(x)$ are local interpolating operators with the same quantum numbers as proton and J/ψ, respectively, and $\alpha, \alpha' = 1, 2$ and $\mu, \mu' = 1, 2, 3$ represent their spin indices [1]. The local interpolating operators are written in terms of quark fields as

$$N_\alpha(x) = \epsilon_{abc}\, u_{\alpha,a}(x) \left(u_b^T(x) C\gamma_5 d_c(x)\right), \tag{3.2}$$

$$\psi_\mu(x) = \bar{c}_d(y)\gamma_\mu c_d(y) \tag{3.3}$$

where color indices are denoted by a, b, c, and d, while Dirac indices are understood implicitly. The charge conjugation matrix is denoted by C. The source operator $\mathcal{J}^{(J^P)\mathrm{wall}}_{\alpha'\mu'}(t_0)$ has the same quantum numbers as the $J/\psi N$ two-particle state. In our study, we employ wall source operators with the Coulomb gauge fixing at $t = t_0$,

$$\mathcal{J}^{(J^P)\mathrm{wall}}_{\alpha'\mu'}(t_0) = \mathcal{P}^{(J)}\mathcal{P}^{(J_z)} N^{\mathrm{wall}}_{\alpha'}(t_0)\psi^{\mathrm{wall}}_{\mu}(t_0), \tag{3.4}$$

where $N^{\mathrm{wall}}(t_0)$ and $\psi^{\mathrm{wall}}(t_0)$ are similar to Eqs. (3.2) and (3.3), but the local quark fields $q(\boldsymbol{x}, t)$ are replaced by the wall quark fields

$$q^{\mathrm{wall}}(t_0) = \sum_{\boldsymbol{x}} q(\boldsymbol{x}, t_0). \tag{3.5}$$

[1] Since we are interested in $J/\psi N$ scattering at low energies, the lower two components of the Dirac spinor are neglected.

Since the wall source operators has zero orbital angular momentum, their parity is determined by the product of the intrinsic parities of nucleon and J/ψ: $P = -1$. In addition, the projections to a desired set of J and J_z are equivalent to projections with respect to the total spin s and its z-component s_z. Note that neither the total spin nor the orbital angular momentum is a good quantum number of the $J/\psi N$ two-particle system: at $t \neq t_0$, the state $\bar{\mathcal{J}}^{(J^P)wall}_{\alpha'\mu'}(t_0)|0\rangle$ contains contribution from partial waves with $l > 0$.

The relation of the correlation function (3.1) to the NBS wave function can be made explicit by inserting the complete set of QCD eigenstates $\mathbf{1} = \sum_n |W_n\rangle \langle W_n|$,

$$C_{\alpha\mu;\alpha'\mu'}(\boldsymbol{r}, t - t_0) = \sum_n \sum_{\boldsymbol{x}} \langle 0 \,|\, N_\alpha(\boldsymbol{r} + \boldsymbol{x}, t)\psi_\mu(\boldsymbol{x}, t) \,|\, W_n\rangle \left\langle W_n \,\middle|\, \bar{\mathcal{J}}^{(J^P)wall}_{\alpha'\mu'}(t_0) \,\middle|\, 0 \right\rangle \tag{3.6}$$

$$= \sum_n \psi^{(J/\psi N)}_{\alpha\mu}(\boldsymbol{r}) A^n_{\alpha'\mu'} e^{-W_n(t-t_0)}, \tag{3.7}$$

where $A^n_{\alpha'\mu'} = \left\langle W_n \,\middle|\, \bar{\mathcal{J}}_{\alpha'\mu'}(0) \,\middle|\, 0 \right\rangle$. If we choose $J^P = 1/2^-$, the NBS wave function is composed of two states: $(l, s) = (0, 1/2)$ and $(2, 3/2)$. Similarly, for $J^P = 3/2^-$, there are three states: $(l, s) = (0, 3/2)$, $(2, 1/2)$, $(2, 3/2)$. In order to extract each of these states, we consider projections to a specific combination of (l, s) for the sink operators. This will be the topic of the next subsection.

The $\eta_c N$ NBS wave function can be constructed in a similar manner as that of $J/\psi N$:

$$C_{\alpha;\alpha'}(\boldsymbol{r}, t - t_0) = \sum_{\boldsymbol{x}} \left\langle 0 \,\middle|\, N_\alpha(\boldsymbol{r} + \boldsymbol{x}, t)\eta(\boldsymbol{x}, t)\bar{\mathcal{J}}^{(J^P)wall}_{\alpha'}(t_0) \,\middle|\, 0 \right\rangle \tag{3.8}$$

$$= \sum_n \psi^{(\eta_c N)}_{\alpha}(\boldsymbol{r}) A^n_{\alpha'} e^{-W_n(t-t_0)}, \tag{3.9}$$

where instead of the J/ψ interpolating operator in Eq. (3.3), we use the η_c operator

$$\eta(x) = \bar{c}_d(y)\gamma_5 c_d(y) \tag{3.10}$$

and the wall source

$$\mathcal{J}^{(J^P)wall}_{\alpha'}(t_0) = \mathcal{P}^{(J)}\mathcal{P}^{(J_z)} N^{wall}_{\alpha'}(t_0)\eta^{wall}(t_0). \tag{3.11}$$

Since the total spin of $\eta_c N$ is 1/2, the orbital angular momentum is unique for a given J^P.

3.1.2 Angular Momentum Projections

The asymptotic form of two-particle wave functions can be classified by the total spin s, the orbital angular momentum l, and the total angular momentum J. They are conveniently denoted by the term symbols $^{2s+1}l_J$, where $l = 0, 1, 2, 3, 4, ...$ are written as $S, P, D, F, G, ...$, *etc.* In Table 3.1, some low-partial wave charmonium-nucleon states are summarized.

In an infinite volume, QCD has the three-dimensional rotational symmetry associated with SO(3) group and parity symmetry. As we move to a finite volume hypercube, they are reduced

to a subgroup, the so-called octahedral group O_h. The properties of O_h are essential for studying the spin-dependent wave functions on the lattice. A cube has rotational symmetry O with 24 elements: 1 identity, 6 rotations by $\pi/2$ about a 4-fold axis, 8 rotations by $2\pi/3$ about a 3-fold axis, 3 rotations by π about a 4-fold axis, and 6 rotations by π about a 2-fold axis. By combining O with group $C_i = \{E, I\}$, where E is identity and I is reflection, we find

$$O_h = O \times C_i. \tag{3.12}$$

The total symmetry group O_h has 48 elements. Any rotationally-invariant quantity in a finite box is represented by the irreducible representations of O_h. The relation between the irreducible representations of O and those of SO(3) is given in Table 3.2. The irreducible representations of O_h is similar to those of O, but with superscript $\pm$, indicating the parity eigenvalue. Physically relevant representations are those with $P = (-1)^l$. For example, the A_1^+ representation of O contains states with $l = 0, 4, \cdots$, while the E^+ representation contains $l = 2, 4, \cdots$. In our study, we assume that the contribution from the states with $l \geq 4$ are negligibly small, so that A_1^+ (E^+) representation contains the S-wave (D-wave) states only.

Projection to a specific irreducible representation Γ^P with parity P can be done by using the character χ_{Γ^P} of Γ^P as

$$P^{(\Gamma^P)} = \frac{d_{\Gamma^P}}{48} \sum_{i=1}^{48} \chi^*_{\Gamma^P}(g_i) D(g_i), \tag{3.13}$$

where g_i is the i-th element of O_h, $D(g_i)$ is the representation matrix of g_i, and d_{Γ^P} is the dimension of Γ^P. Note that, since our wall source operator has fixed parity $P = -$, the projection to representation Γ^P of O_h gives the same result as that to the corresponding representation Γ of O. Therefore, we have

$$P^{(\Gamma^P)} = P^{(\Gamma)} = \frac{d_\alpha}{24} \sum_{i=1}^{24} \chi^*_{\Gamma}(g_i) D(g_i). \tag{3.14}$$

The projection to the S-wave orbital angular momentum corresponds to the projection to the A_1 representation of O upto small corrections from the states with $l \geq 4$. Similarly, the projection to D-wave orbital angular momentum can be realized by the projection to the E representation with corrections from $l \geq 4$ [2]. Applying them to the $J/\psi N$ correlation function

Table 3.1: Some low-partial wave charmonium-nucleon states classified by s, l, and J.

	$s = 1/2$		$s = 3/2$	
J	$l = even$	$l = odd$	$l = even$	$l = odd$
1/2	${}^2S_{1/2}$	${}^2P_{1/2}$	${}^4D_{1/2}$	${}^4P_{1/2}$
3/2	${}^2D_{3/2}$	${}^2P_{3/2}$	${}^4S_{3/2}$, ${}^4D_{3/2}$	${}^4P_{3/2}$, ${}^4F_{3/2}$
5/2	${}^2D_{5/2}$	${}^2F_{5/2}$	${}^4D_{5/2}$, ${}^4G_{5/2}$	${}^4P_{5/2}$, ${}^4F_{5/2}$

[2] Although the T_2 representation of O also contains $l = 2, 4, \cdots$, we only consider the E representation for D-wave.

$C_{\alpha\mu;\alpha'\mu'}(\boldsymbol{r},t)$ or the η_c correlation function $C_{\alpha;\alpha'}(\boldsymbol{r},t)$, one finds

$$P^{(\Gamma(l))}C_{\alpha\mu;\alpha'\mu'}(\boldsymbol{r},t) = \frac{d_{\Gamma(l)}}{24}\sum_{i=1}^{24}\chi^*_{\Gamma(l)}(g_i)C_{\alpha\mu;\alpha'\mu'}(g_i^{-1}\boldsymbol{r},t), \tag{3.15}$$

$$P^{(\Gamma(l))}C_{\alpha;\alpha'}(\boldsymbol{r},t) = \frac{d_{\Gamma(l)}}{24}\sum_{i=1}^{24}\chi^*_{\Gamma(l)}(g_i)C_{\alpha;\alpha'}(g_i^{-1}\boldsymbol{r},t), \tag{3.16}$$

with $\Gamma(l=0)=A_1$ and $\Gamma(l=2)=E$.

Projection of the total spin s is somewhat more detailed. As in Table 3.1, the total spin of the charmonium-nucleon systems are either $1/2$ or $3/2$. The spin-$1/2$ representation for the identity element $E \in O_h$ is the unit matrix of rank $2s+1=2$,

$$D^{(1/2)}(E) = \mathbf{1}_2. \tag{3.17}$$

As far as the irreducible representations in Table 3.1 are concerned, a rotation by 2π around any axis, say $\bar{E}$, is identical to E:

$$D^{(A_1/A_2/E/T_1/T_2)}(\bar{E}) = D^{(A_1/A_2/E/T_1/T_2)}(E). \tag{3.18}$$

On the contrary, a representation matrix in the spin-$1/2$ basis transforms to its negative through $\bar{E}$:

$$D^{(1/2)}(\bar{E}) = -D^{(1/2)}(E). \tag{3.19}$$

Although E and $\bar{E}$ are identical with respect to coordinate rotation, the representation matrix for spin-$1/2$ basis are different between E and $\bar{E}$. These half-integer spin bases are described by double-valued representations of the rotation group O. There are three double-valued irreducible representations in O: $E_{1/2}$, $G_{3/2}$, and $E_{5/2}$, corresponding to the state with $s=1/2$, $s=3/2$, and $s=5/2$, respectively. The projection of the total spin is therefore achieved by the projection to the corresponding double-valued representation $\Gamma(s)$ of O as

$$P^{(\Gamma(s))}C_{\alpha\mu;\alpha'\mu'}(\boldsymbol{r},t) = \frac{d_{\Gamma(s)}}{24}\sum_{i=1}^{24}\chi^*_{\Gamma(s)}(g_i)D^{(1/2)}_{\alpha\beta}(g_i)D^{(1)}_{\mu\nu}(g_i)C_{\beta\nu;\alpha'\mu'}(\boldsymbol{r},t), \tag{3.20}$$

$$P^{(\Gamma(s))}C_{\alpha;\alpha'}(\boldsymbol{r},t) = \frac{d_{\Gamma(s)}}{24}\sum_{i=1}^{24}\chi^*_{\Gamma(s)}(g_i)D^{(1/2)}_{\alpha\beta}(g_i)C_{\beta;\alpha'}(\boldsymbol{r},t), \tag{3.21}$$

with $\Gamma(s=1/2)=E_{1/2}$, $\Gamma(s=3/2)=G_{3/2}$, and $\Gamma(s=5/2)=E_{5/2}$. Similarly, the projection of the total angular momentum for the wall source operator is realized by

$$P^{(\Gamma(J))}C_{\alpha\mu;\alpha'\mu'}(\boldsymbol{r},t) = \frac{d_{\Gamma(J)}}{24}\sum_{i=1}^{24}\chi^*_{\Gamma(J)}(g_i)C_{\alpha\mu;\beta'\nu'}(g_i^{-1}\boldsymbol{r},t)D^{(1/2)\dagger}_{\beta'\alpha'}(g_i)D^{(1)\dagger}_{\nu'\nu}(g_i), \tag{3.22}$$

$$P^{(\Gamma(J))}C_{\alpha;\alpha'}(\boldsymbol{r},t) = \frac{d_{\Gamma(J)}}{24}\sum_{i=1}^{24}\chi^*_{\Gamma(J)}(g_i)C_{\alpha;\beta'}(g_i^{-1}\boldsymbol{r},t)D^{(1/2)\dagger}_{\beta'\alpha'}(g_i). \tag{3.23}$$

3.1.3 Spin Operators and Eigenstates

In this subsection, we discuss the structures of correlation functions $\psi^{(J/\psi N)}_{\alpha\mu}(\boldsymbol{r})$ and $\psi^{(\eta_c N)}_{\alpha}(\boldsymbol{r})$ in a SO(3) symmetric case.

The operators acting on the spinor space are the Pauli matrices,

$$\sigma_1 = \begin{pmatrix} 0 & 1 \\ 1 & 0 \end{pmatrix}, \quad \sigma_2 = \begin{pmatrix} 0 & -i \\ i & 0 \end{pmatrix}, \quad \sigma_3 = \begin{pmatrix} 1 & 0 \\ 0 & -1 \end{pmatrix}. \tag{3.24}$$

They form an orthogonal basis for the Hilbert space of all 2-by-2 matrices together with the unit matrix

$$\mathbf{1}_2 = \begin{pmatrix} 1 & 0 \\ 0 & 1 \end{pmatrix}. \tag{3.25}$$

The third component, σ_3, has eigenvalues ± 1, and the corresponding eigenstates are:

$$|+\rangle_{1/2} = \begin{pmatrix} 1 \\ 0 \end{pmatrix}, \tag{3.26}$$

$$|-\rangle_{1/2} = \begin{pmatrix} 0 \\ 1 \end{pmatrix}. \tag{3.27}$$

The J/ψ spin is expressed by matrices

$$\Sigma_1 = \begin{pmatrix} 0 & 0 & 0 \\ 0 & 0 & -i \\ 0 & +i & 0 \end{pmatrix}, \quad \Sigma_2 = \begin{pmatrix} 0 & 0 & +i \\ 0 & 0 & 0 \\ -i & 0 & 0 \end{pmatrix}, \quad \Sigma_3 = \begin{pmatrix} 0 & -i & 0 \\ +i & 0 & 0 \\ 0 & 0 & 0 \end{pmatrix}, \tag{3.28}$$

which are Hermitian, unitary and traceless, and satisfy the commutation relations $[\Sigma_i, \Sigma_j] = i\epsilon_{ijk}\Sigma_k$, just like the Pauli matrices. Also, we define the 3-by-3 unit Matrix as

$$\mathbf{1}_3 = \begin{pmatrix} 1 & 0 & 0 \\ 0 & 1 & 0 \\ 0 & 0 & 1 \end{pmatrix}. \tag{3.29}$$

Table 3.2: The number of irreducible representations of O in the irreducible representations of SO(3) with angular momentum $l \leq 4$. $P = (-1)^l$ is the parity eigenvalue.

l	P	A_1	A_2	E	T_1	T_2
0	+	1	0	0	0	0
1	-	0	0	0	1	0
2	+	0	0	1	0	1
3	-	0	1	0	1	1
4	+	1	0	1	1	1

To form an orthogonal basis for the Hilbert space of 3-by-3 matrices, additional five independent matrices are needed. They are given by the second-order traceless symmetric matrices

$$P_{ij}^{(2)}(S) \equiv S_{ij} = \frac{1}{2}\{S_i, S_j\} - \frac{1}{3}\vec{S}^2\delta_{ij}, \tag{3.30}$$

with $(i,j) = (1,2),(2,3),(3,1),(1,1),(2,2)$. The eigenvalues of Σ_3 are ± 1 and 0, with eigenstates

$$|+1\rangle_1 = -\frac{1}{\sqrt{2}}\begin{pmatrix}1\\ i\\ 0\end{pmatrix}, \tag{3.31}$$

$$|-1\rangle_1 = \frac{1}{\sqrt{2}}\begin{pmatrix}1\\ -i\\ 0\end{pmatrix}, \tag{3.32}$$

$$|0\rangle_1 = \begin{pmatrix}0\\ 0\\ 1\end{pmatrix}. \tag{3.33}$$

By using these operators, total spin operator of the $J/\psi N$ system is defined as

$$\boldsymbol{S} = \frac{\boldsymbol{\sigma}}{2} \otimes \mathbf{1}_3 + \mathbf{1}_2 \otimes \boldsymbol{\Sigma}. \tag{3.34}$$

The total spin of the $J/\psi N$ system is either 1/2 or 3/2; therefore $\boldsymbol{S}^2$ has eigenvalues 3/4 and 15/4. All our spin operators $\boldsymbol{s} = \boldsymbol{\sigma}/2, \boldsymbol{\Sigma}, \boldsymbol{S}$ and their eigenstates $|m\rangle_s$ are such that they satisfy the relations

$$s_\pm |m\rangle_s = (s_1 \pm i s_2)|m\rangle_s = \sqrt{(s \mp m)(s \pm m + 1)}\,|m \pm 1\rangle_s, \tag{3.35}$$

$$s_3 |m\rangle_s = m\,|m\rangle_s. \tag{3.36}$$

Now, the $J/\psi N$ wave function $\psi_{\alpha\mu}^{(J/\psi N)}(\boldsymbol{r})$ can be written as a 2-by-3 matrix by arranging α in rows and μ in columns:

$$\psi^{(J/\psi N)}(\boldsymbol{r}) = \{\psi_{\alpha\mu}(\boldsymbol{r})\} = \begin{pmatrix}\psi_{11}(\boldsymbol{r}) & \psi_{12}(\boldsymbol{r}) & \psi_{13}(\boldsymbol{r})\\ \psi_{21}(\boldsymbol{r}) & \psi_{22}(\boldsymbol{r}) & \psi_{23}(\boldsymbol{r})\end{pmatrix}. \tag{3.37}$$

In the case of infinite volume, we find that the angular dependence of the $J/\psi N$ wave function is described as by a spin harmonics $\mathcal{Y}_{J,J_z}^{(l,s)}(\hat{\boldsymbol{r}})$ as

$$\psi^{(J/\psi N)}(\boldsymbol{r}) = u_l(r)\mathcal{Y}_{J,J_z}^{(l,s)}(\hat{\boldsymbol{r}}), \tag{3.38}$$

where J, J_z, l, and s are the total angular momentum and its z-component, the orbital angular momentum, and the total spin, respectively. The spin harmonics is a known 2-by-3 matrix. In Appendix. A, the specific forms of the $J/\psi N$ spin harmonics are summerized.

3.1.4 Numerical Results of the NBS Wave Functions

Our numerical lattice QCD calculations are performed on the (2+1) flavor full QCD configurations generated by the CP-PACS and JLQCD collaborations [38]. They are generated with the renormalization-group improved gauge action and a non-perturbatively $\mathcal{O}(a)$ improved clover quark action at $\beta = 6/g^2 = 1.90$, corresponding to lattice spacing of $a = 0.0907(13)$ fm in both spatial and temporal directions. The lattice size is $L^3T = 32^3 \times 64$. The spatial volume is $La = 2.902(42)$ fm, which should be large enough to accommodate the charmonium-nucleon interactions. In the present study, we employ the set of configurations with the heaviest light-quark masses, corresponding to pion mass of $m_\pi = 700(2)$ MeV. We employ the relativistic heavy quark (RHQ) action for charm quark to avoid the leading $\mathcal{O}(m_c a^n)$ with arbitrary order n and the next-to-leading $\mathcal{O}(m_c a)^n (a\Lambda_{\rm QCD})$ discretization errors [39]. We use the RHQ parameters in Ref. [40], which are determined to reproduce the experimental charmed-hadron masses with almost-physical light quark masses and the relativistic dispersion relation for the spin-averaged 1S charmonium state. The quark propagators are calculated with point sink operator and the wall source operator at Euclidean time $t = t_0$. The periodic boundary condition is imposed on the spatial directions, while the Dirichlet boundary condition is imposed on the temporal direction to avoid backward propagation at $t - t_0 = 32a$. An average over 32 different wall source positions are considered to improve statistics. The statistical uncertainties are estimated by the jackknife method with bin size 57. We have confirmed that a change of the bin size to 21 or 19 do not show visible difference in the estimated error.

We first see the masses of the nucleon and the charmonia. They can be extracted from a two-point correlation function averaged over all spatial points,

$$C_2(t - t_0) = \sum_{\boldsymbol{x}} \left\langle 0 \left| A(\boldsymbol{x}, t) \bar{A}^{\rm wall}(t_0) \right| 0 \right\rangle , \tag{3.39}$$

where $A(\boldsymbol{x}, t)$ is an interpolating field operator for the hadron. The temporal correlation of $C_2(t)$ at large t is $\exp(-mt)$, so that the effective mass,

$$am_{\rm eff}(t) = \log \left(\frac{C_2(t)}{C_2(t+a)} \right) , \tag{3.40}$$

tends to the hadron mass ma as $t \to \infty$.

In Fig. 3.1, we show the effective masses of N (Panel (a)), J/ψ and η_c (Panel (b)). As we expect, we see a plateau region at large t in all cases. The masses are estimated by fitting the two-point correlation functions by a single exponent. We find that $m_N = 1585.3 \pm 16.1$ MeV, $m_{J/\psi} = 3139.1 \pm 11.7$ MeV, and $m_{\eta_c} = 3021.9 \pm 9.2$ MeV, which are extracted in ranges $t = 14 - 19$, $t = 15 - 18$, and $t = 15 - 18$, respectively. While the nucleon mass is very different from the experimental value of $m_N^{\rm (exp)} = 938.3$ MeV, the charmonium masses are much closer to $m_{J/\psi}^{\rm (exp)} = 3096.9$ MeV and $m_{\eta_c}^{\rm (exp)} = 2983.9$ MeV. Therefore, we expect that the effects of unphysical quark masses are mainly from the light quarks.

The masses calculated here are used for to calculate the potentials in the HAL QCD method. In addition, the exponential factors in the time-dependent Schrödinger-like Eq. (2.60)

is replaced by the two-point correlation functions as

$$R(\boldsymbol{r}, t) = C(\boldsymbol{r}, t) \times e^{(m_1+m_2)t} \tag{3.41}$$

$$\simeq C(\boldsymbol{r}, t) / \left(C_2^{(N)}(t) C_2^{(c\bar{c})}(t) \right), \tag{3.42}$$

because statistical noise may be canceled between the correlation functions. This replacement is justified when $C_2(t)$ are expressed by a single exponent, so that we use $t \geq 15$ to calculate the potentials.

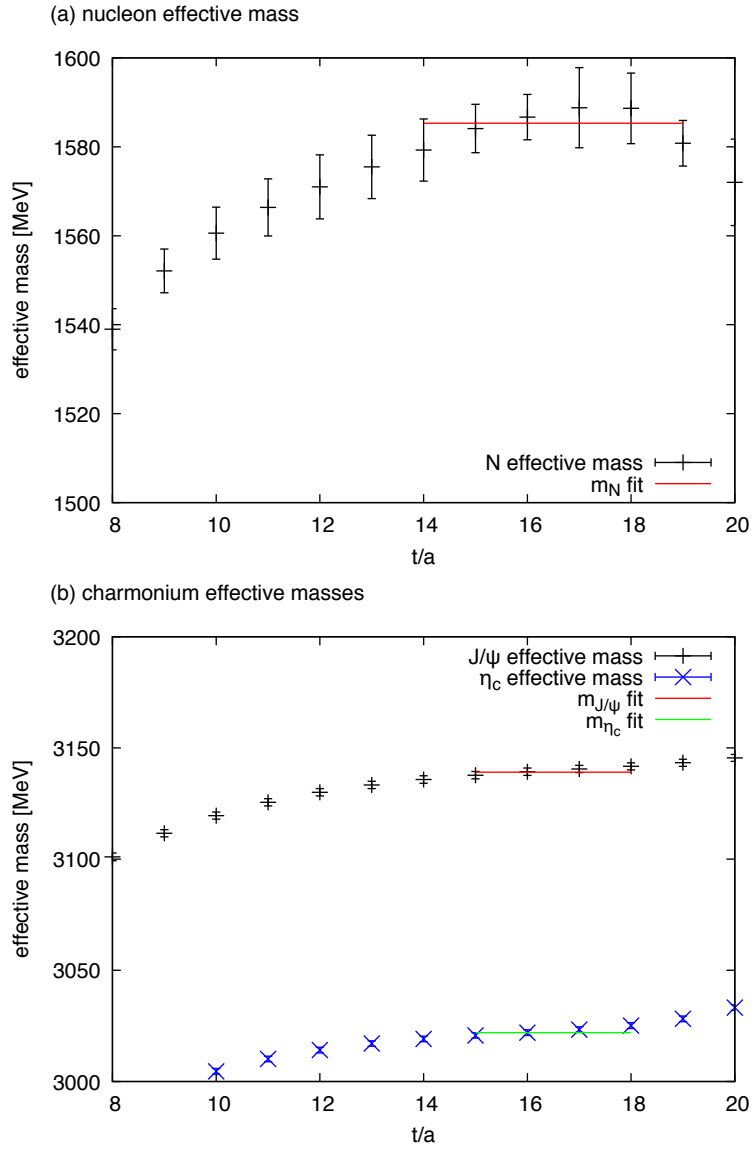

Figure 3.1: The effective masses for (a) nucleon and (b) J/ψ and η_c. The fit value and the fit range are also shown.

In Fig. 3.2, we show the $J/\psi N$ four-point correlation functions divided by the spin harmonics,

$$\mathcal{P}^{(l,s)}_{J,J_z} C(\boldsymbol{r}, t) / \mathcal{Y}^{(l,s)}_{J,J_z}(\hat{\boldsymbol{r}}), \tag{3.43}$$

where $\mathcal{P}$ is a product of projection operators to the representation of O_h corresponding to angular momentum (J, J_z, l, m). They roughly correspond to the radial wave function of the ground state, if the violation of SO(3) symmetry and the excited state contributions are both neglected. We see that the S-wave states ${}^2S_{1/2}$ and ${}^4S_{3/2}$ are calculated with good precision. However, the D-wave states, ${}^4D_{1/2}$, ${}^2D_{3/2}$, and ${}^4D_{3/2}$ have 10^{-3} times smaller signal and large error. The poor D-wave signal is probably because of the use of wall source operator, which allows only the S-wave state at $t = t_0$. Also, since SO(3) is not a precise symmetry on the lattice, the four-point correlation function does not have the angular dependence of $\mathcal{Y}^{(l,s)}_{J,J_z}(\hat{\boldsymbol{r}})$ on the lattice; as a result, the quantity (3.43) is not a single-valued function of r. We would need a more sophisticated analysis to extract D-wave states with precision. Nevertheless we can mainly utilize the signals for the S-wave states in our study, since S-wave states play a central role for low-energy scattering. In particular, we consider the S-wave effective central potentials in the next section.

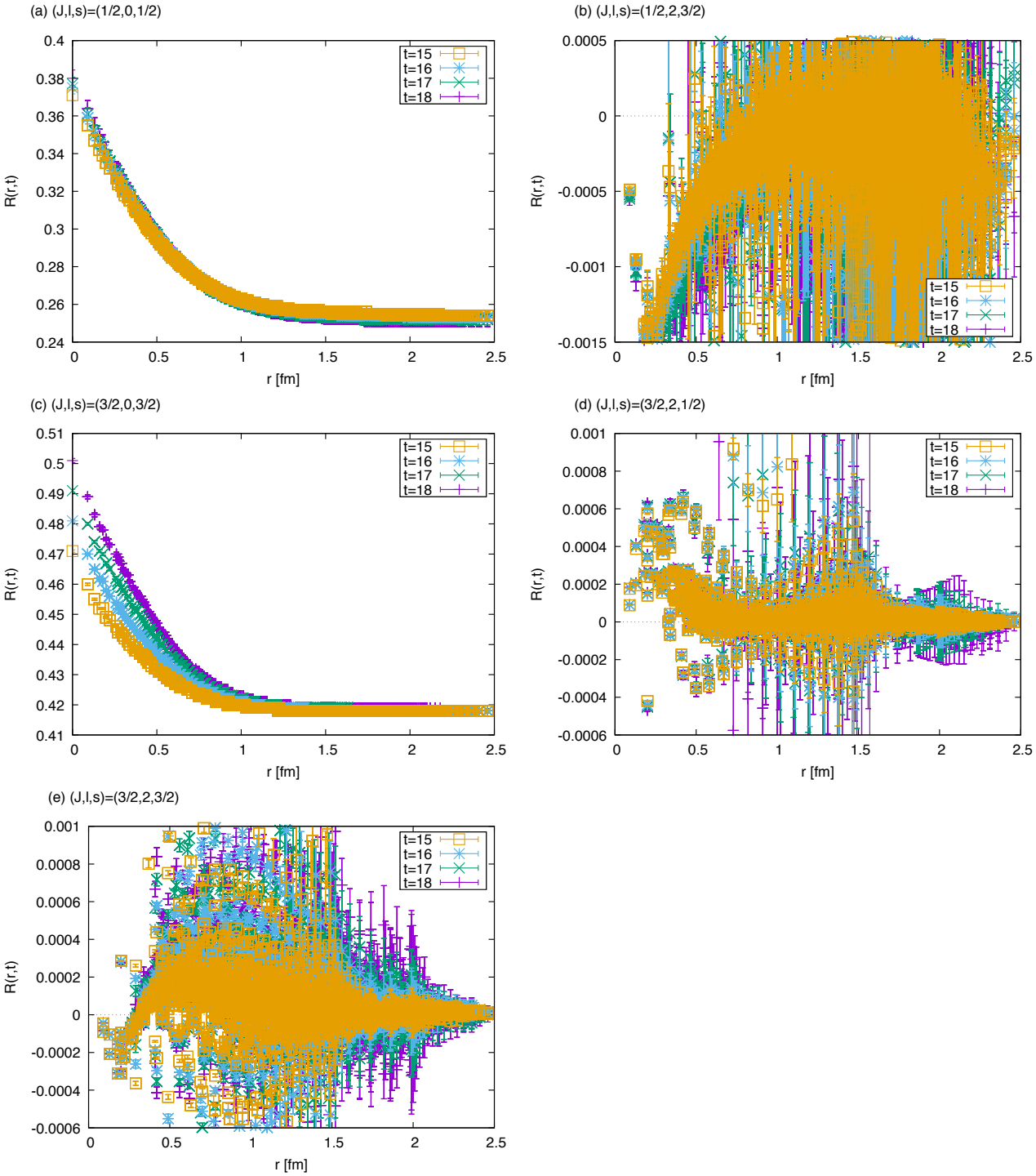

Figure 3.2: R-correlators with $J_z = J$.

3.2 Low-energy Scattering with Effective Central Potentials

3.2.1 Effective Central Potentials

In general, the initial and final states can have different orbital angular momentum or total spin, since the rotational symmetry preserves the combination $\boldsymbol{J} = \boldsymbol{l} + \boldsymbol{s}$, but not $\boldsymbol{l}$ or $\boldsymbol{s}$. The $\eta_c N$ system with $J^P = 1/2^-$ is the only allowed state because the total spin of $\eta_c N$ is 1/2 and only $l = 0$ contributes to $J^P = 1/2^-$. However, there are two $J/\psi N$ states with $J^P = 1/2^-$ ($^2S_{1/2}$ and $^4D_{1/2}$) and three states with $J^P = 3/2^-$ ($^4S_{3/2}$, $^2D_{3/2}$, and $^4D_{3/2}$). The states with the same J mix through the spin-dependent forces. In this section, we temporarily avoid treating such transition forces in a straightforward manner; instead we calculate an effective central potential, which is defined through

$$\left(\frac{1+3\delta^2}{8\mu}\frac{\partial^2}{\partial t^2} + \frac{\partial}{\partial t} + H_0\right)\mathcal{P}^{(l,s)}_{J,J_z} R(\boldsymbol{r},t) = V_{\text{eff}}(r)\mathcal{P}^{(l,s)}_{J,J_z} R(\boldsymbol{r},t), \tag{3.44}$$

where $V_{\text{eff}}(r)$ is a scalar function. The transition effects through loop diagrams are effectively introduced in V_{eff}. We consider the S-wave effective central potentials to study low-energy charmonium-nucleon scattering. Note that the $J = 1/2$ state of the $J/\psi N$ can couple to the S-wave $\eta_c N$ state through channel mixing; however, we assume the channel mixing is small, since it involves re-arrangement of the charm quark spins.

In Fig. 3.3, we show the effective central potentials for the S-wave charmonium-nucleon states, *i.e.*, $\eta_c N$, $J/\psi N$ with $J = 1/2$, and $J/\psi N$ with $J = 3/2$. They are determined at Euclidean time $(t - t_0)/a = 15$. The charmonium-nucleon interactions show qualitatively similar behavior in all the three cases: they are all attractive and finite-ranged. This is expected from the QCD van der Waals interaction model, where the non-perturbative QCD effects of the light quarks and gluons are considered to be independent of the charmonium states.

To take a closer look, Fig. 3.3 shows that the strength of the interaction depends on the channels. Among the three, the $\eta_c N$ has the weakest attraction. The strength of the $J/\psi N$ interaction depends on the total angular momentum J: the effective central potential with $J = 1/2$ is more attractive than that with $J = 3/2$. Since the $\eta_c N$ interaction is weaker than the $J/\psi N$ interaction with both $J = 1/2$ and $J = 3/2$, one will infer that the weaker attraction of $\eta_c N$ originates from the properties of charmonia, rather than kinematical effects. The reduced masses of the $J/\psi N$ and the $\eta_c N$ are $\mu_{J/\psi N} = 1052.4\,\text{MeV}$ and $\mu_{\eta_c N} = 1038.9\,\text{MeV}$, respectively, and are only different by 1.3%. This is far insufficient to explain the $\sim 20\%$ difference seen in Fig. 3.3. Phenomenologically, the charmonium-nucleon interaction can be described by a chromoelectric dipole interaction in Eq. (1.3), where the chromoelectric polarizability α behaves as the cube of the non-relativistic charmonium Bohr radius. The smaller radius of η_c compared to that of J/ψ suggests that α tends to be smaller, so that the $\eta_c N$ interaction is weaker than the $J/\psi N$.

The splitting of the $J/\psi N$ effective central potentials is due to the spin-dependent forces. The spin-dependent forces are small, since they are suppressed by factors of $\mathcal{O}(1/m_c)$. They

arise due to interference of the chromoelectric dipole and the chromomagnetic quadrupole [25]. In the next chapter, we will derive the general form of the $J/\psi N$ interaction with spin-dependent forces at the lowest order of the derivative expansion, and determine them on the lattice.

The assumptions used to derive Eq. (3.44) are: (1) the four-point correlation function is dominated by elastic charmonium-nucleon two-body states, and (2) the derivative expansion of the non-local and energy-independent HAL QCD potential converges such that low-energy scattering is described by a local potential $U(\boldsymbol{r}, \boldsymbol{r}') = V_0(r)\delta^3(\boldsymbol{r} - \boldsymbol{r}')$. If both of the two assumptions are satisfied, the resulting potential is independent of Euclidean time t. In Fig. 3.4, we show the effective central potentials determined at $(t - t_0)/a = 15 - 20$. No significant t-dependence is observed in all the three cases. Therefore, we conclude that the two assumptions are satisfied already at $(t - t_0)/a = 15$. The good agreement of the effective central potentials from different t shows that systematic error in our calculation is sufficiently small.

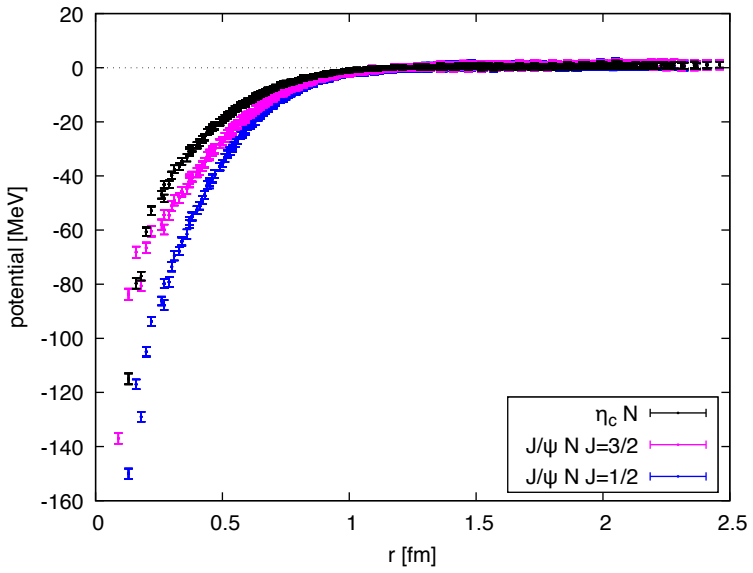

Figure 3.3: The S-wave effective central potentials at $(t - t_0)/a = 15$: (magenta) $J/\psi N$ with $J = 3/2$, (blue) $J/\psi N$ with $J = 3/2$, and (black) $\eta_c N$.

3.2.2 Scattering Phase Shift

The effective central potentials are short-ranged, so that they receive small finite volume effects. The extrapolation to the infinite volume can thus be easily done, by fitting the potentials with a function that quickly goes to zero as r increases. We employ a fit by two Gaussian functions, $V_{\rm eff}(r) = \sum_{n=1,2} a_n \exp(-v_n r^2)$ in all cases. Then it can be used to solve the effective radial

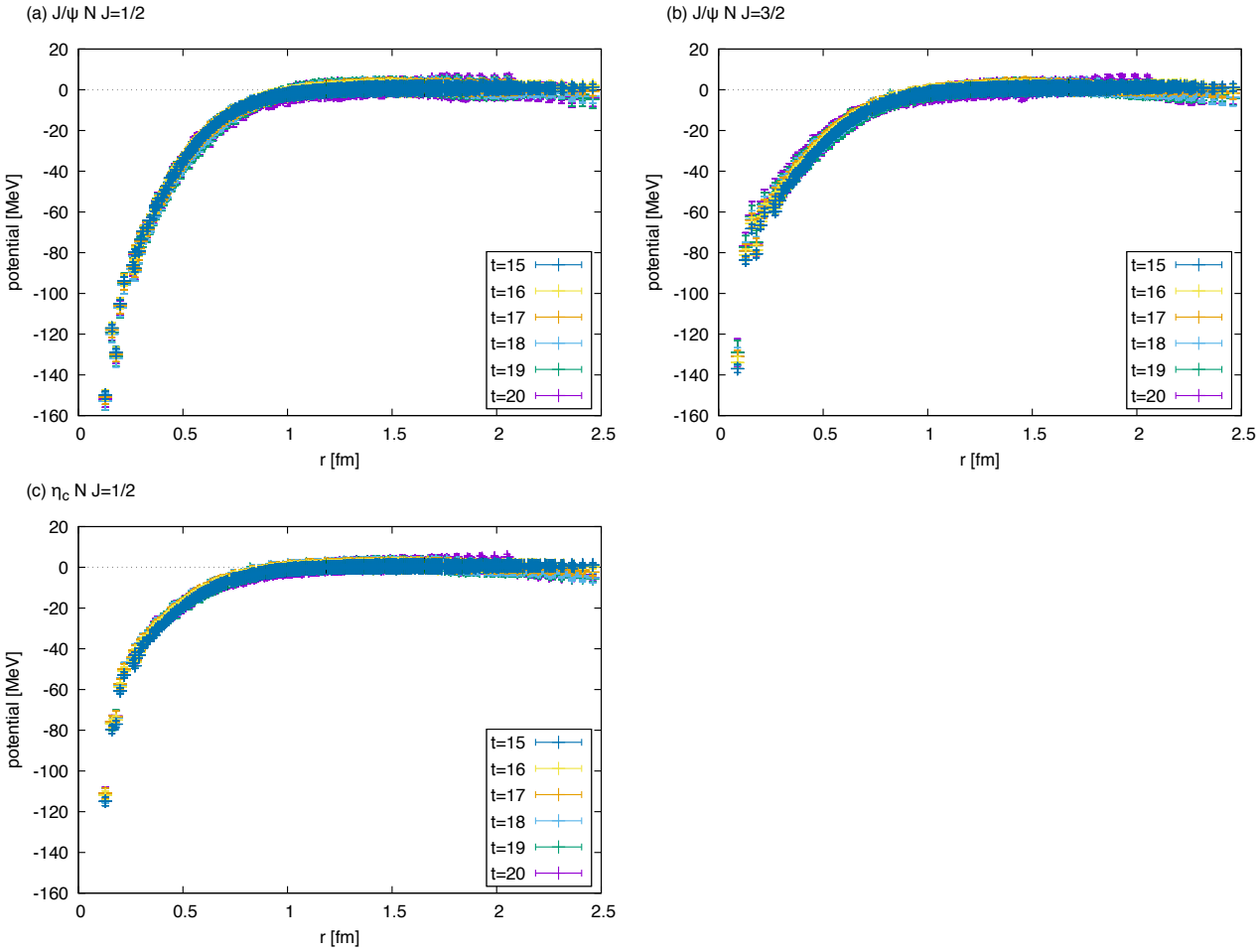

Figure 3.4: The Euclidean time t dependence of the effective central potentials: (a) $J/\psi N$ with $J = 1/2$, (b) $J/\psi N$ with $J = 3/2$, and (c) $\eta_c N$.

Schrödinger equation

$$\left[-\frac{1}{2\mu}\frac{\partial^2}{\partial r^2} + V_{\text{eff}}(r)\right]\phi_0(r;E) = E\phi_0(r;E). \tag{3.45}$$

At large r the solution behaves like

$$\phi_0(r;E) = \frac{i}{2}\left(F_0(k)\hat{h}_0^{(-)}(kr) - F_0^*(k)\hat{h}_0^{(+)}(kr)\right), \tag{3.46}$$

where $E = k^2/(2\mu)$. The $l = 0$ Riccati-Hankel functions are $\hat{h}_0^{(\pm)}(kr) = \exp(\pm kr)$. The Jost function can be extracted from ϕ_0 and $\phi_0' = (\partial/\partial r)\phi_0$ as

$$\begin{pmatrix}\phi_0(r;E)\\ \phi_0'(r;E)\end{pmatrix} = \frac{i}{2}\begin{pmatrix}\hat{h}_0^{(-)}(kr) & -\hat{h}_0^{(+)}(kr)\\ k\hat{h}_0'^{(-)}(kr) & -k\hat{h}_0'^{(+)}(kr)\end{pmatrix}\begin{pmatrix}F_0(k)\\ F_0^*(k)\end{pmatrix}. \tag{3.47}$$

The scattering phase shift is them given by

$$s_0(k) = \frac{F_0^*(k)}{F_0(k)} = \exp(2i\delta_0(k)). \tag{3.48}$$

In Fig. 3.5, we show the phase shifts as a function of the center of mass energy E. We find no charmonium-nucleon bound state. Also, the low-energy S-matrix elements are well parameterized by the scattering length a and the effective range r, defined through the effective range expansion

$$k \cot \delta_0(k) = \frac{1}{a} + \frac{r}{2}k^2 + \mathcal{O}(k^4). \tag{3.49}$$

Neglecting the $\mathcal{O}(k^4)$, the scattering length and the effective range of the S-wave charmonium-nucleon interactions are obtained as in Table. 3.3, where the error is for statistical uncertainties only.

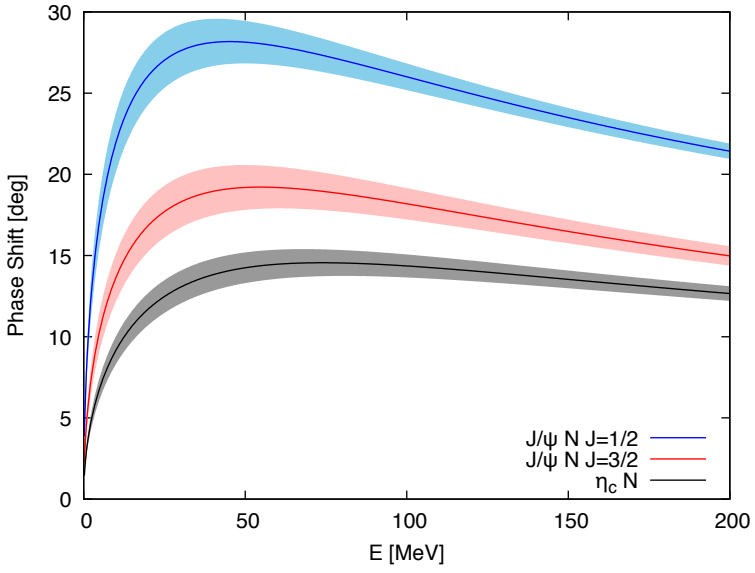

Figure 3.5: The phase shifts calculated from the S-wave effective potentials at $(t - t_0)/a = 15$. (magenta) $J/\psi N$ with $J = 3/2$, (blue) $J/\psi N$ with $J = 3/2$, and (black) $\eta_c N$.

Table 3.3: The scattering length and the effective range from the effective central potentials.

channel	a[fm]	r[fm]
$J/\psi N,\ J = 1/2$	0.656 ± 0.071	1.105 ± 0.016
$J/\psi N,\ J = 3/2$	0.380 ± 0.048	1.476 ± 0.039
$\eta_c N$	0.246 ± 0.026	1.703 ± 0.045

3.2.3 Comparison with Previous Results

Some previous works of the charmonium-nucleon interactions on the lattice have been reported. The first lattice QCD calculation is given by Yokokawa *et al.* [41]. They have utilized Lüscher's method to calculate the scattering length of $\eta_c N$ and spin-averaged $J/\psi N$ by the quenched lattice QCD to find $a_{\eta_c N} = 0.70 \pm 0.66\,\mathrm{fm}$ and $a_{J/\psi N} = 0.71 \pm 0.48\,\mathrm{fm}$ where chiral extrapolation is made to the physical quark masses. Another study by Lüscher's method is done by Kawanai and Sasaki also by the quenched lattice QCD [42]. They have found that $a_{\eta_c N} \sim 0.25\,\mathrm{fm}$ and $a_{J/\psi N} \sim 0.35\,\mathrm{fm}$. They have used three quark masses corresponding to $m_\pi = 0.64$, 0.72, and $0.87\,\mathrm{GeV}$, but no significant difference is observed in the scattering lengths. Although these results have relatively large uncertainties, they roughly agree with our results in Table. 3.3.

Kawanai and Sasaki have also calculated the charmonium-nucleon potentials by the time-independent HAL QCD method and with the quenched approximation [42, 43]. In Fig. 3.6 we show their results of the $\eta_c N$ and the spin-averaged $J/\psi N$ effective central potentials at $m_\pi = 640\,\mathrm{MeV}$. They are qualitatively similar to our results. To make a more clear comparison, in Fig. 3.7, we re-plot our results (Fig. 3.3) in the scale of Fig. 3.6. Then it is apparent that all of our potentials have stronger attraction than the corresponding potential by Kawanai and Sasaki. The difference is because Kawanai and Sasaki used the old HAL QCD method, where the ground-state saturation is assumed. In actual situations the ground-state saturation is very hard to achieve, so that the use of the time-dependent method is necessary. It seems that they have underestimated the short-range part of the potential.

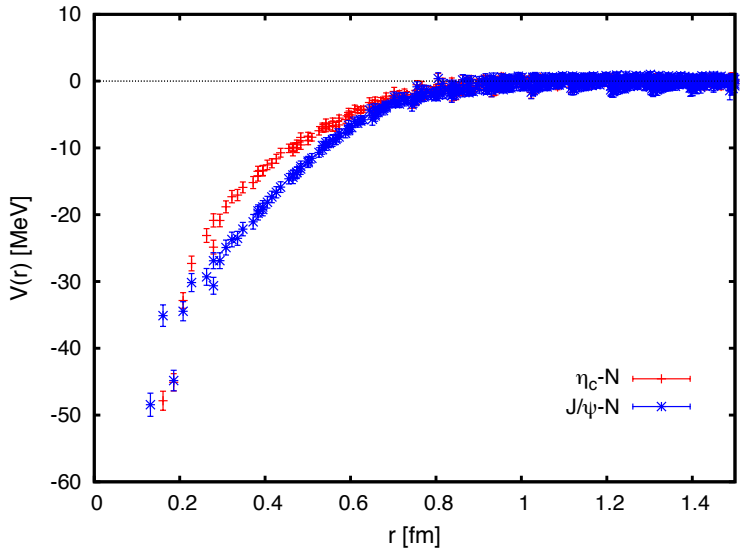

Figure 3.6: The effective central potentials for the $\eta_c N$ and the spin-averaged $J/\psi N$ by the time-independent HAL QCD method at $m_\pi = 640\,\mathrm{MeV}$. The figure is taken from Ref. [43].

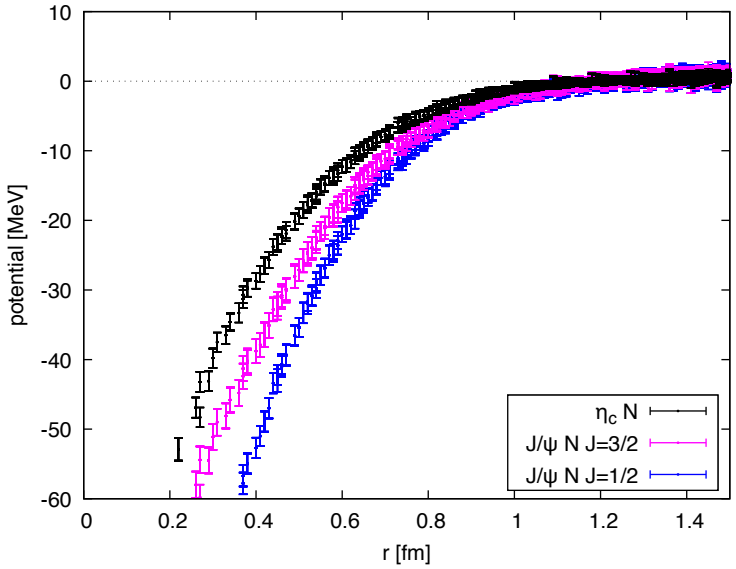

Figure 3.7: Our effective central potentials in Fig. 3.3 shown in the scale of Fig. 3.6.

3.3 Spin-Dependent forces of the $J/\psi N$ Interaction

3.3.1 Okubo-Marshak Decomposition

In this subsection, we follow the arguments of Okubo-Marshak [44] to derive the $J/\psi N$ interaction at the lowest order of the derivative expansion. The general form of the $J/\psi N$ 2-body potential is

$$V = V(\boldsymbol{r}_1, \boldsymbol{r}_2, \boldsymbol{p}_1, \boldsymbol{p}_2, \boldsymbol{\sigma}, \boldsymbol{\Sigma}, \boldsymbol{\tau}, t), \tag{3.50}$$

where $\boldsymbol{r}_{1,2}$ and $\boldsymbol{p}_{1,2}$ are the positions and momenta of N or J/ψ, $\boldsymbol{\sigma}$ is the spin of N, $\boldsymbol{\Sigma}$ is the spin of J/ψ, $\boldsymbol{\tau}$ is the isospin of N, and t is the time of interaction. We require V to satisfy the following 6 conditions:

1. Energy-momentum conservation
   Energy conservation is satisfied when V does not depend on t explicitly. Momentum conservation implies that V should be translationally invariant. Thus we have

   $$V = V(\boldsymbol{r}, \boldsymbol{p}_1, \boldsymbol{p}_2, \boldsymbol{\sigma}, \boldsymbol{\Sigma}, \boldsymbol{\tau}), \tag{3.51}$$

   with $\boldsymbol{r} = \boldsymbol{r}_1 - \boldsymbol{r}_2$.

2. Galilei covariance
   It is assumed that V is independent of the center of mass momentum of the system, so that

   $$V = V(\boldsymbol{r}, \boldsymbol{q}, \boldsymbol{\sigma}, \boldsymbol{\Sigma}, \boldsymbol{\tau}), \tag{3.52}$$

   with $\boldsymbol{q} = \boldsymbol{p}_1 - \boldsymbol{p}_2$.

3. Isospin invariance
   Since $m_u \sim m_d$, QCD has approximate SU(2) symmetry with respect to flavor-space rotation. Thus V should not depend on $\boldsymbol{\tau}$:

   $$V = V(\boldsymbol{r}, \boldsymbol{q}, \boldsymbol{\sigma}, \boldsymbol{\Sigma}) \tag{3.53}$$

4. Conservation of total angular momentum
   Rotational invariance of V is required. thus V is a scalar function of the vectors $\boldsymbol{r}$, $\boldsymbol{q}$, $\boldsymbol{\sigma}$, and $\boldsymbol{\Sigma}$.

5. Parity invariance
   Strong interaction preserves parity. Thus

   $$V(\boldsymbol{r}, \boldsymbol{q}, \boldsymbol{\sigma}, \boldsymbol{\Sigma}) = V(-\boldsymbol{r}, -\boldsymbol{q}, \boldsymbol{\sigma}, \boldsymbol{\Sigma}). \tag{3.54}$$

6. Time reversal invariance
   Strong interaction preserves time-reversal symmetry. Thus

$$V(\boldsymbol{r},\, \boldsymbol{q},\, \boldsymbol{\sigma},\, \boldsymbol{\Sigma}) = V(\boldsymbol{r},\, -\boldsymbol{q},\, -\boldsymbol{\sigma},\, -\boldsymbol{\Sigma}). \tag{3.55}$$

In the following, we do not consider the momentum q dependence of the potential, since we are interested in the low-energy $J/\psi N$ scattering. We find that there are four operators allowed:

$$\mathbf{1} = \mathbf{1}_2 \otimes \mathbf{1}_3, \tag{3.56}$$
$$\boldsymbol{\sigma} \cdot \boldsymbol{\Sigma}, \tag{3.57}$$
$$S_{12} \equiv 3(\hat{\boldsymbol{r}} \cdot \boldsymbol{\sigma})(\hat{\boldsymbol{r}} \cdot \boldsymbol{\Sigma}) - \boldsymbol{\sigma} \cdot \boldsymbol{\Sigma}, \tag{3.58}$$
$$T_{12} \equiv 3(\hat{\boldsymbol{r}} \cdot \boldsymbol{\Sigma})^2 - \boldsymbol{\Sigma}^2, \tag{3.59}$$

where $\hat{\boldsymbol{r}} = \boldsymbol{r}/|\boldsymbol{r}|$. Note that the normalization of operators S_{12} and T_{12} is changed from that of the traceless symmetric tensor $P^{(2)}_{ij}$ by a factor of 3. Therefore, the general form of the $J/\psi N$ interaction is given as

$$V = V_0(r) + V_s(r)\boldsymbol{\sigma} \cdot \boldsymbol{\Sigma} + V_{T1}(r)S_{12} + V_{T2}(r)T_{12}. \tag{3.60}$$

3.3.2 Matrix Elements of the Potential

Since the $J/\psi N$ potential in Eq. (3.60) is rotationally-invariant, it preserves the total angular momentum J and J_z. The total spin operator (3.34) is related to $\boldsymbol{\sigma} \cdot \boldsymbol{\Sigma}$ as

$$\boldsymbol{S}^2 = \left(\frac{1}{2}\boldsymbol{\sigma} + \boldsymbol{\Sigma}\right)^2 \tag{3.61}$$
$$= \boldsymbol{\sigma} \cdot \boldsymbol{\Sigma} + \frac{1}{4}\boldsymbol{\sigma}^2 + \boldsymbol{\Sigma}^2 \tag{3.62}$$
$$= \boldsymbol{\sigma} \cdot \boldsymbol{\Sigma} + \frac{11}{4}, \tag{3.63}$$

since $\boldsymbol{\sigma}^2 = 3$ and $\boldsymbol{\Sigma}^2 = 2$. Therefore, the spin-spin force $V_s(r)$ preserves the total spin s and the orbital angular momentum l:

$$\left[\boldsymbol{S}^2, \boldsymbol{\sigma} \cdot \boldsymbol{\Sigma}\right] = 0, \tag{3.64}$$
$$\left[\boldsymbol{L}^2, \boldsymbol{\sigma} \cdot \boldsymbol{\Sigma}\right] = 0. \tag{3.65}$$

The operator $\hat{\boldsymbol{r}} \cdot \boldsymbol{\sigma}$ can be written in terms of the ladder operators $\sigma_\pm = \sigma_1 \pm i\sigma_2$ as

$$\hat{\boldsymbol{r}} \cdot \boldsymbol{\sigma} = \sigma_1 \sin\theta\cos\phi + \sigma_2 \sin\theta\sin\phi + \sigma_3\cos\theta \tag{3.66}$$
$$= \frac{1}{2}(\sigma_+ + \sigma_-)\sin\theta\cos\phi + \frac{1}{2i}(\sigma_+ - \sigma_-)\sin\theta\sin\phi + \sigma_3\cos\theta \tag{3.67}$$
$$= \frac{1}{2}\sigma_+ \sin\theta e^{-i\theta} + \frac{1}{2}\sigma_- \sin\theta e^{+i\theta} + \sigma_3\cos\theta. \tag{3.68}$$

Similarly, $\hat{\boldsymbol{r}} \cdot \boldsymbol{\Sigma}$ becomes

$$\hat{\boldsymbol{r}} \cdot \boldsymbol{\Sigma} = \frac{1}{2}\Sigma_+ \sin\theta e^{-i\theta} + \frac{1}{2}\Sigma_- \sin\theta e^{+i\theta} + \Sigma_3 \cos\theta. \tag{3.69}$$

One can show that the operators $(\hat{\boldsymbol{r}} \cdot \boldsymbol{\sigma})^2$ and $(\hat{\boldsymbol{r}} \cdot \boldsymbol{\Sigma})^2$ does not commute with neither $\boldsymbol{S}^2$ nor $\boldsymbol{L}^2$. Therefore, the tensor forces $V_{T1}(r)$ and $V_{T2}(r)$ does not preserve either s or l:

$$\left[\boldsymbol{S}^2, S_{12}\right] \neq 0, \tag{3.70}$$
$$\left[\boldsymbol{L}^2, S_{12}\right] \neq 0, \tag{3.71}$$
$$\left[\boldsymbol{S}^2, T_{12}\right] \neq 0, \tag{3.72}$$
$$\left[\boldsymbol{L}^2, T_{12}\right] \neq 0. \tag{3.73}$$

Note that, the two-nucleon tensor operator

$$S_{12}^{(NN)} = 3\,(\hat{\boldsymbol{r}} \cdot \boldsymbol{\sigma}_1)\,(\hat{\boldsymbol{r}} \cdot \boldsymbol{\sigma}_2) - \boldsymbol{\sigma}_1 \cdot \boldsymbol{\sigma}_2, \tag{3.74}$$

couples the S- and D-wave states in the spin-triplet channel, but does preserve the total spin:

$$\left[\boldsymbol{S}^2, S_{12}^{(NN)}\right] = 0, \tag{3.75}$$
$$\left[\boldsymbol{L}^2, S_{12}^{(NN)}\right] \neq 0. \tag{3.76}$$

The reason for the total spin conservation in the NN case is that they are identical particles, and the tensor operator $S_{12}^{(NN)}$ is symmetric under permutation of the particles. Of course this is not the case for $J/\psi N$.

We focus on the $J/\psi N$ two-particle scattering with minus parity. There are five such states, two with $J = 1/2$ and three with $J = 3/2$: ${}^2S_{1/2}$, ${}^4D_{1/2}$, ${}^4S_{3/2}$, ${}^2D_{3/2}$, ${}^4D_{3/2}$. (See Table 3.1). Since the potential in Eq. (3.60) is rotationally invariant, the matrix elements of the potential does not depend on J_z. One can calculate the matrix elements of the potential by using the properties of the angular momentum operators in Eqs. (3.35) and (3.36), and the recursion formulae for the spherical harmonics,

$$\sin\theta e^{-i\phi} Y_l^m = +\sqrt{\frac{(l-m+1)(l-m+2)}{(2l+1)(2l+3)}} Y_{l+1}^{m-1} - \sqrt{\frac{(l+m-1)(l+m)}{(2l-1)(2l+1)}} Y_{l-1}^{m-1}, \tag{3.77}$$

$$\sin\theta e^{+i\phi} Y_l^m = -\sqrt{\frac{(l+m+1)(l+m+2))}{(2l+1)(2l+3)}} Y_{l+1}^{m+1} + \sqrt{\frac{(l-m-1)(l-m))}{(2l-1)(2l+1)}} Y_{l-1}^{m+1}, \tag{3.78}$$

$$\cos\theta Y_l^m = +\sqrt{\frac{(l-m+1)(l+m+1)}{(2l+1)(2l+3)}} Y_{l+1}^{m} + \sqrt{\frac{(l-m)(l+m)}{(2l-1)(2l+1)}} Y_{l-1}^{m}. \tag{3.79}$$

Then one finds the following results:

$$\left\langle {}^2S_{\frac{1}{2}} \middle| V \middle| {}^2S_{\frac{1}{2}} \right\rangle = V_0 - 2V_s \tag{3.80}$$

$$\left\langle {}^4D_{\frac{1}{2}} \middle| V \middle| {}^4D_{\frac{1}{2}} \right\rangle = V_0 + V_s - 2V_{T1} - V_{T2} \tag{3.81}$$

$$\left\langle {}^2S_{\frac{1}{2}} \middle| V \middle| {}^4D_{\frac{1}{2}} \right\rangle = -\sqrt{2}V_{T1} + \sqrt{2}V_{T2} \tag{3.82}$$

$$\left\langle {}^4S_{\frac{3}{2}} \middle| V \middle| {}^4S_{\frac{3}{2}} \right\rangle = V_0 + V_s \tag{3.83}$$

$$\left\langle {}^2D_{\frac{3}{2}} \middle| V \middle| {}^2D_{\frac{3}{2}} \right\rangle = V_0 - 2V_s \tag{3.84}$$

$$\left\langle {}^4D_{\frac{3}{2}} \middle| V \middle| {}^4D_{\frac{3}{2}} \right\rangle = V_0 + V_s \tag{3.85}$$

$$\left\langle {}^4S_{\frac{3}{2}} \middle| V \middle| {}^2D_{\frac{3}{2}} \right\rangle = +V_{T1} - V_{T2} \tag{3.86}$$

$$\left\langle {}^4S_{\frac{3}{2}} \middle| V \middle| {}^4D_{\frac{3}{2}} \right\rangle = +2V_{T1} + V_{T2} \tag{3.87}$$

$$\left\langle {}^2D_{\frac{3}{2}} \middle| V \middle| {}^4D_{\frac{3}{2}} \right\rangle = -V_{T1} + V_{T2} \tag{3.88}$$

These results can be summerized as in Tables 3.4 and 3.5. Since V is Hermite, the matrix elements are symmetric under the permutation of the initial and the final states.

Table 3.4: Matrix elements of the $J/\psi N$ potential for $J = \frac{1}{2}$

${}^{2s+1}L_J$	${}^2S_{1/2}$	${}^4D_{1/2}$
${}^2S_{1/2}$	$V_0 - 2V_s$	$-\sqrt{2}V_{T1} + \sqrt{2}V_{T2}$
${}^4D_{1/2}$		$V_0 + V_s - 2V_{T1} - V_{T2}$

Table 3.5: Matrix elements of the $J/\psi N$ potential for $J = \frac{3}{2}$.

${}^{2s+1}L_J$	${}^4S_{3/2}$	${}^2D_{3/2}$	${}^4D_{3/2}$
${}^4S_{3/2}$	$V_0 + V_s$	$V_{T1} - V_{T2}$	$2V_{T1} + V_{T2}$
${}^2D_{3/2}$		$V_0 - 2V_s$	$-V_{T1} + V_{T2}$
${}^4D_{3/2}$			$V_0 + V_s$

The heavy-quark spin symmetry indicates that the J/ψ spin-flipping effects are suppressed by $\mathcal{O}(1/m_c)$. Thus we naïvely expect that

$$V_0(r) = \mathcal{O}(1), \tag{3.89}$$

$$V_s(r) = \mathcal{O}(1/m_c), \tag{3.90}$$

$$V_{T1}(r) = \mathcal{O}(1/m_c), \tag{3.91}$$

$$V_{T2}(r) = \mathcal{O}(1/m_c^2). \tag{3.92}$$

3.3.3 Determination of the Potential

In this section we discuss how to determine the potentials $V_0(r), V_s(r), V_{T1}(r), V_{T2}(r)$ by lattice QCD calculations. For this purpose we first discuss the case when the system has rotational SO(3) symmetry.

If the derivative expansion converges at the lowest order, the Schrödinger-like equation in the time-dependent HAL QCD method becomes

$$\left(\frac{1+3\delta^2}{8\mu}\frac{\partial^2}{\partial t^2}+\frac{\partial}{\partial t}+H_0\right)R_{\alpha\mu}(\boldsymbol{r},t) = V_0(r)R_{\alpha\mu}(\boldsymbol{r},t)+V_s(r)\left(\boldsymbol{\sigma}\cdot\boldsymbol{\Sigma}R\right)_{\alpha\mu}(\boldsymbol{r},t)+V_{T1}(r)\left(S_{12}R\right)_{\alpha\mu}(\boldsymbol{r},t)+V_{T2}(r)\left(T_{12}R\right)_{\alpha\mu}(\boldsymbol{r},t), \tag{3.93}$$

where α and μ are the spin indices of nucleon and J/ψ, respectively. As discussed in the previous section, we have five different combinations of (J,l,s). The total angular momentum quantum numbers J and J_z are fixed at $t=0$. In this study, we use the states with $J_z=+J$ to determine the potentials. We denote the projection operators of J, J_z, l, and s as $\mathcal{P}_i$ $(i=1,2,3,4,5)$:

$$\mathcal{P}_1 = \mathcal{P}_{J=1/2}\mathcal{P}_{J_z=+1/2}\mathcal{P}_{l=0}\mathcal{P}_{s=1/2}, \tag{3.94}$$
$$\mathcal{P}_2 = \mathcal{P}_{J=1/2}\mathcal{P}_{J_z=+1/2}\mathcal{P}_{l=2}\mathcal{P}_{s=3/2}, \tag{3.95}$$
$$\mathcal{P}_3 = \mathcal{P}_{J=3/2}\mathcal{P}_{J_z=+3/2}\mathcal{P}_{l=0}\mathcal{P}_{s=3/2}, \tag{3.96}$$
$$\mathcal{P}_4 = \mathcal{P}_{J=3/2}\mathcal{P}_{J_z=+3/2}\mathcal{P}_{l=2}\mathcal{P}_{s=1/2}, \tag{3.97}$$
$$\mathcal{P}_5 = \mathcal{P}_{J=3/2}\mathcal{P}_{J_z=+3/2}\mathcal{P}_{l=2}\mathcal{P}_{s=3/2}, \tag{3.98}$$

which corresponds to projections to ${}^2S_{1/2}$, ${}^4D_{1/2}$, ${}^4S_{3/2}$, ${}^2D_{3/2}$, and ${}^4D_{3/2}$, respectively. By applying them from the left of Eq. (3.93), we get five linearly-independent equations

$$\left(\frac{1+3\delta^2}{8\mu}\frac{\partial^2}{\partial t^2}+\frac{\partial}{\partial t}+H_0\right)\left(\mathcal{P}_iR\right)_{\alpha\mu}(\boldsymbol{r},t) = V_0(r)\left(\mathcal{P}_iR\right)_{\alpha\mu}(\boldsymbol{r},t)+V_s(r)\left(\mathcal{P}_i\boldsymbol{\sigma}\cdot\boldsymbol{\Sigma}R\right)_{\alpha\mu}(\boldsymbol{r},t) + V_{T1}(r)\left(\mathcal{P}_iS_{12}R\right)_{\alpha\mu}(\boldsymbol{r},t)+V_{T2}(r)\left(\mathcal{P}_iT_{12}R\right)_{\alpha\mu}(\boldsymbol{r},t), \tag{3.99}$$

where we have utilized the fact that $\mathcal{P}_i$ commutes with the scalar functions $V_0(r)$, $V_s(r)$, $V_{T1}(r)$, $V_{T2}(r)$, and operators H_0 and $\partial/\partial t$, but not with operators with spin indices. There are four unknown functions and we have five linearly-independent equations. We can choose four of these equations labeled by $i=(i_1,i_2,i_3,i_4)$ and combine them to a matrix form

$$\boldsymbol{K}_{\alpha\mu}(\boldsymbol{r},t) = M_{\alpha\mu}(\boldsymbol{r},t)\boldsymbol{v}(r), \tag{3.100}$$

where we have introduced simplified notations

$$\boldsymbol{K}_{\alpha\mu}(\boldsymbol{r},t) = \begin{pmatrix} \left(\frac{1+3\delta^2}{8\mu}\frac{\partial^2}{\partial t^2} + \frac{\partial}{\partial t} + H_0\right)(\mathcal{P}_{i_1}R)_{\alpha\mu}(\boldsymbol{r},t) \\ \left(\frac{1+3\delta^2}{8\mu}\frac{\partial^2}{\partial t^2} + \frac{\partial}{\partial t} + H_0\right)(\mathcal{P}_{i_2}R)_{\alpha\mu}(\boldsymbol{r},t) \\ \left(\frac{1+3\delta^2}{8\mu}\frac{\partial^2}{\partial t^2} + \frac{\partial}{\partial t} + H_0\right)(\mathcal{P}_{i_3}R)_{\alpha\mu}(\boldsymbol{r},t) \\ \left(\frac{1+3\delta^2}{8\mu}\frac{\partial^2}{\partial t^2} + \frac{\partial}{\partial t} + H_0\right)(\mathcal{P}_{i_4}R)_{\alpha\mu}(\boldsymbol{r},t) \end{pmatrix}, \tag{3.101}$$

$$M_{\alpha\mu}(\boldsymbol{r},t) = \begin{pmatrix} (\mathcal{P}_{i_1}R)_{\alpha\mu}(\boldsymbol{r},t) & (\mathcal{P}_{i_1}\boldsymbol{\sigma}\cdot\boldsymbol{\Sigma}R)_{\alpha\mu}(\boldsymbol{r},t) & (\mathcal{P}_{i_1}S_{12}R)_{\alpha\mu}(\boldsymbol{r},t) & (\mathcal{P}_{i_1}T_{12}R)_{\alpha\mu}(\boldsymbol{r},t) \\ (\mathcal{P}_{i_2}R)_{\alpha\mu}(\boldsymbol{r},t) & (\mathcal{P}_{i_2}\boldsymbol{\sigma}\cdot\boldsymbol{\Sigma}R)_{\alpha\mu}(\boldsymbol{r},t) & (\mathcal{P}_{i_2}S_{12}R)_{\alpha\mu}(\boldsymbol{r},t) & (\mathcal{P}_{i_2}T_{12}R)_{\alpha\mu}(\boldsymbol{r},t) \\ (\mathcal{P}_{i_3}R)_{\alpha\mu}(\boldsymbol{r},t) & (\mathcal{P}_{i_3}\boldsymbol{\sigma}\cdot\boldsymbol{\Sigma}R)_{\alpha\mu}(\boldsymbol{r},t) & (\mathcal{P}_{i_3}S_{12}R)_{\alpha\mu}(\boldsymbol{r},t) & (\mathcal{P}_{i_3}T_{12}R)_{\alpha\mu}(\boldsymbol{r},t) \\ (\mathcal{P}_{i_4}R)_{\alpha\mu}(\boldsymbol{r},t) & (\mathcal{P}_{i_4}\boldsymbol{\sigma}\cdot\boldsymbol{\Sigma}R)_{\alpha\mu}(\boldsymbol{r},t) & (\mathcal{P}_{i_4}S_{12}R)_{\alpha\mu}(\boldsymbol{r},t) & (\mathcal{P}_{i_4}T_{12}R)_{\alpha\mu}(\boldsymbol{r},t) \end{pmatrix}, \tag{3.102}$$

$$\boldsymbol{v}(r) = \begin{pmatrix} V_0(r) \\ V_s(r) \\ V_{T1}(r) \\ V_{T2}(r) \end{pmatrix}. \tag{3.103}$$

Then we can solve this equation by multiplying the inverse of $M(\boldsymbol{r},t)$ from the left at each spatial points $\boldsymbol{r}$:

$$\boldsymbol{v}(r) = M^{-1}_{\alpha\mu}(\boldsymbol{r},t)\boldsymbol{K}_{\alpha\mu}(\boldsymbol{r},t). \tag{3.104}$$

The choice of four projection operators $i = (i_1, i_2, i_3, i_4)$ is arbitrary. Five such choices are possible, and all of them should give the identical results within statistical error if there is no source of systematic error. Therefore, this can be a check of a necessary condition that our three assumptions are satisfied: (1) Elastic-state saturation is achieved at Euclidean time t. (2) The derivative expansion converges such that low-energy $J/\psi N$ scattering can be described by the lowest-order potential in Eq. (3.60). (3) The contamination of states with $l \geq 4$ in the irreducible representations of O_h is negligibly small. Moreover, when the above conditions are all satisfied, the left-hand side of Eq. (3.104) is not dependent on t, although the right-hand side can be ostensibly.

Now we are set to consider the spin indices $\alpha = 1, 2$ and $\mu = 1, 2, 3$ of the correlation functions. In principle, Eq. (3.100) consists of $6 = 2 \times 3$ components, and we need to consider a proper linear combination of them in order to determine the potentials with less systematic error. The spin structure of a function $f(\boldsymbol{r},t)$ with spin indices α and μ and angular momentum J, J_z, l, and s (corresponding to $\mathcal{P}_iR$, $\mathcal{P}_iS_{12}R$, *etc.*) has the form

$$f_{\alpha\mu}(\boldsymbol{r},t) = \sum_{n=0}^{\infty} A^n e^{-W_n t} f_l^n(r) \left(\mathcal{Y}^{(l,s)}_{J,J_z}\right)_{\alpha\mu}(\hat{\boldsymbol{r}}), \tag{3.105}$$

where n labels the QCD energy eigenvalues W_n, A^n is a constant in $\mathbb{C}$, and $\mathcal{Y}^{(l,s)}_{J,J_z}(\hat{\boldsymbol{r}})$ is the known spinor harmonics (see Appendix A). For example, the spinor harmonics with $(J, J_z, l, s) =$

$(1/2, +1/2, 0, 1/2)$ is

$$\mathcal{Y}^{(0,1/2)}_{1/2,+1/2}(\hat{\boldsymbol{r}}) = \frac{1}{\sqrt{12\pi}} \begin{pmatrix} 0 & 0 & -1 \\ -1 & -i & 0 \end{pmatrix}. \tag{3.106}$$

We find that the components $(\alpha, \mu) = (1,3)$, $(2,1)$, $(2,2)$ have the same entries upto irrelevant overall factor. We can use one of these components to determine the potential. On the contrary, the other components $(\alpha, \mu) = (1,1)$, $(1,2)$, $(2,3)$ are zero, so that they do not contain information of the interaction. The D-wave states have somewhat more complicated structure. In the case of $(J, J_z, l, s) = (1/2, +1/2, 2, 3/2)$, we get

$$\mathcal{Y}^{(2,3/2)}_{1/2,+1/2}(\hat{\boldsymbol{r}}) = \frac{1}{\sqrt{60}} \begin{pmatrix} -\sqrt{3}Y_2^{+1}(\hat{\boldsymbol{r}}) - \sqrt{3}Y_2^{-1}(\hat{\boldsymbol{r}}) & i\sqrt{3}Y_2^{+1}(\hat{\boldsymbol{r}}) + i\sqrt{3}Y_2^{-1}(\hat{\boldsymbol{r}}) & 2\sqrt{2}Y_2^{0}(\hat{\boldsymbol{r}}) \\ 2\sqrt{3}Y_2^{+2}(\hat{\boldsymbol{r}}) - \sqrt{2}Y_2^{0}(\hat{\boldsymbol{r}}) & -i2\sqrt{3}Y_2^{+2}(\hat{\boldsymbol{r}}) - i\sqrt{2}Y_2^{0}(\hat{\boldsymbol{r}}) & -2\sqrt{3}Y_2^{+1}(\hat{\boldsymbol{r}}) \end{pmatrix} \tag{3.107}$$

$$= \frac{1}{\sqrt{24\pi}} \begin{pmatrix} 3i\hat{y}\hat{z} & 3\hat{y}\hat{z} & -\hat{x}^2 - \hat{y}^2 + 2\hat{z}^2 \\ 2\hat{x}^2 - \hat{y}^2 - \hat{z}^2 + 3i\hat{x}\hat{y} & -\hat{x}^2 + 2\hat{y}^2 - \hat{z}^2 - 3i\hat{x}\hat{y} & 3\hat{x}\hat{z} + 3i\hat{y}\hat{z} \end{pmatrix}, \tag{3.108}$$

where $Y_l^m(\hat{\boldsymbol{r}})$ are the spherical harmonics and $\hat{\boldsymbol{r}} = \boldsymbol{r}/|\boldsymbol{r}| = (\hat{x}, \hat{y}, \hat{z})$. Equation (3.108) shows that, if we take an equation from the $(\alpha, \beta) = (1,2)$ component for example, it provides a null result at points on the xy-plane or the xz-plane. Similarly, if we take the $(1,3)$ component, it provides a null results at points with $\boldsymbol{r} = (\pm n, \pm n, \pm n)$ (with $n \in \mathbb{Z}$, any double sign). In order to determine the potential as many points as possible, we need to combine these equations from different spin components. This can be done by multiplying $\mathcal{Y}^{(l,s)*}_{J,J_z}(\hat{\boldsymbol{r}})$ from the left of Eq. (3.105), so that

$$\sum_{\alpha=1,2}\sum_{\mu=1,2,3} \left(\mathcal{Y}^{(l,s)*}_{J,J_z}\right)_{\alpha\mu}(\hat{\boldsymbol{r}}) f_{\alpha\mu}(\boldsymbol{r},t) = \sum_{n=0}^{\infty} A^n e^{-W_n t} u_l^n(r) \sum_{\alpha=1,2}\sum_{\mu=1,2,3} \left| \left(\mathcal{Y}^{(l,s)}_{J,J_z}\right)_{\alpha\mu}(\hat{\boldsymbol{r}}) \right|^2, \tag{3.109}$$

which is zero only at the origin $\boldsymbol{r} = 0$, because of the orthogonality of the spherical harmonics. We introduce a matrix

$$Y_{\alpha\mu}(\hat{\boldsymbol{r}}) = \begin{pmatrix} \left(\mathcal{Y}^{(l_1,s_1)}_{J,J_z}\right)_{\alpha\mu}(\hat{\boldsymbol{r}}) & & & \\ & \left(\mathcal{Y}^{(l_2,s_2)}_{J,J_z}\right)_{\alpha\mu}(\hat{\boldsymbol{r}}) & & \\ & & \left(\mathcal{Y}^{(l_3,s_3)}_{J,J_z}\right)_{\alpha\mu}(\hat{\boldsymbol{r}}) & \\ & & & \left(\mathcal{Y}^{(l_4,s_4)}_{J,J_z}\right)_{\alpha\mu}(\hat{\boldsymbol{r}}) \end{pmatrix}, \tag{3.110}$$

where (l_j, s_j) $(j = 1,2,3,4)$ correspond to the orbital angular momentum l and the total spin s of the projection operator P_{i_j}. By multiplying this from the left of Eq. (3.100) and summing over α and μ, we get

$$Y^*(\hat{\boldsymbol{r}}) \cdot \boldsymbol{K}(\boldsymbol{r},t) = Y^*(\hat{\boldsymbol{r}}) \cdot M(\boldsymbol{r},t)\boldsymbol{v}(r), \tag{3.111}$$

where $(\cdot)$ denotes the inner product in the spin space:

$$Y^*(\hat{\boldsymbol{r}}) \cdot \boldsymbol{K}(\boldsymbol{r}, t) = \sum_{\alpha=1,2} \sum_{\mu=1,2,3} Y^*_{\alpha\mu}(\hat{\boldsymbol{r}}) \boldsymbol{K}_{\alpha\mu}(\boldsymbol{r}, t). \tag{3.112}$$

The solution to Eq. (3.111) is

$$\boldsymbol{v}(r) = \left(Y^*(\hat{\boldsymbol{r}}) \cdot M(\boldsymbol{r}, t)\right)^{-1} \left(Y^*(\hat{\boldsymbol{r}}) \cdot \boldsymbol{K}(\boldsymbol{r}, t)\right). \tag{3.113}$$

This is a linear combination of Eqs. (3.104) with different (α, μ) components. The results are null only at $\boldsymbol{r} = 0$.

3.3.4 Numerical Results of the Spin-Dependent $J/\psi N$ Potentials

Although in principle we can consider five combinations of the projection operators to determine the potential, in actual calculations the signals of D-wave state are much smaller than the S-wave signals (See Fig. 3.2). Therefore, here we consider two combinations: case 1: ($\mathcal{P}_1$, $\mathcal{P}_3$, $\mathcal{P}_4$, $\mathcal{P}_5$), and case 2: ($\mathcal{P}_1$, $\mathcal{P}_2$, $\mathcal{P}_3$, $\mathcal{P}_5$), to utilize the S-wave signals.

In Fig. 3.8, we show the spin-dependent potentials in the two cases. We see that the central force is dominant as expected, whereas the spin-spin force gives sizeable contribution. The tensor forces are both small compared to the former two. No significant difference can be seen for the central and the spin-spin forces between case 1 and case 2. For the tensor forces, we see small difference.

In order to compare with the S-wave effective central potentials, we first note that the diagonal matrix element of the potential for the ${}^2S_{1/2}$ and the ${}^4S_{3/2}$ states are $V_0(r) - 2V_s(r)$ and $V_0(r) + V_s(r)$, respectively. Therefore, the stronger attraction of the $J = 1/2$ channel can be explained by the fact that $V_s(r) > 0$. In Fig. 3.9, we show the result for the linear combinations $V_0(r) - 2V_s(r)$ and $V_0(r) + V_s(r)$. It shows excellent agreement with the effective central potentials in Fig. 3.3. The spin-spin force is the origin of the hyperfine splitting between the $J = 1/2$ and the $J = 3/2$ states. In the context of the QCD van der Waals interaction, this is related to the interference of chromoelectric dipole $E1$ and the chromomagnetic quadrupole $M2$ transitions. It will be interesting to compare our lattice results with a phenomenological calculation of the hyperfine splitting.

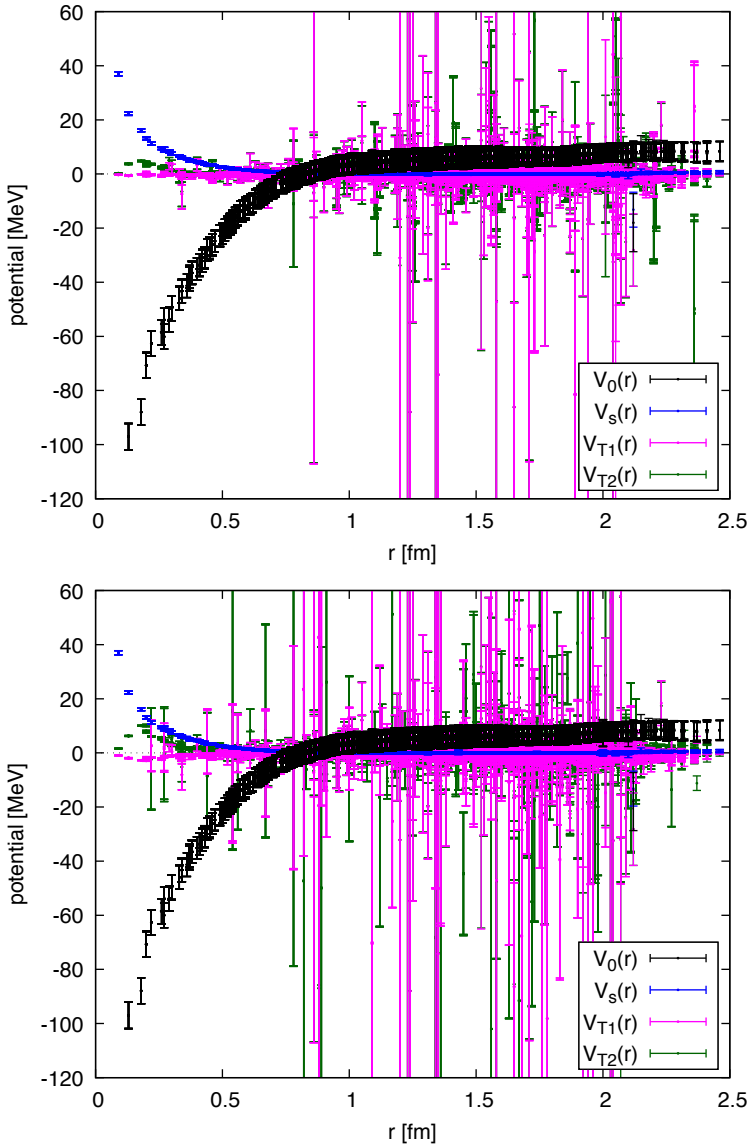

Figure 3.8: The spin-dependent forces of the $J/\psi N$ interaction at $(t-t_0)/a = 15$. (upper) case 1, (lower) case 2. When calculating the matrix inversion in Eq. (3.113), there are some points with condition number larger than 10^{10} since they involve large systematic uncertainties.

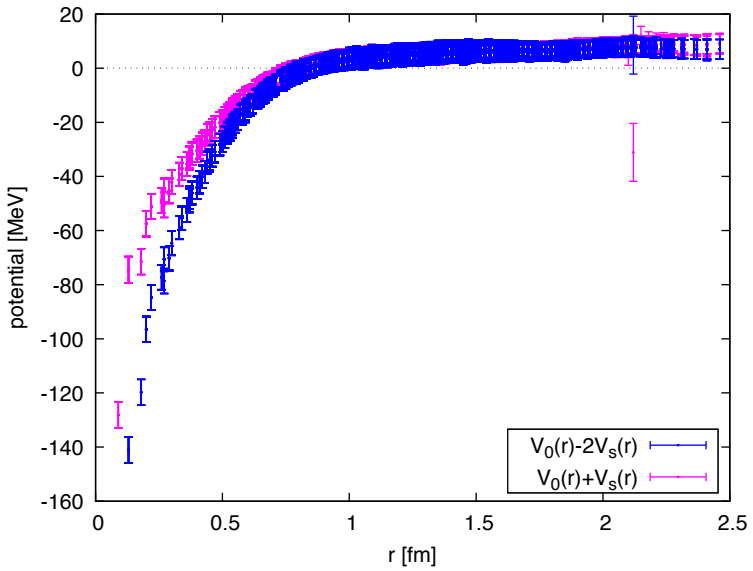

Figure 3.9: Linear combinations of the central and the spin-spin forces: $V_0(r) - 2V_s(r)$ and $V_0(r) + V_s(r)$, which correspond to the diagonal matrix element of the states ${}^2S_{1/2}$ and ${}^4S_{3/2}$, respectively.

Chapter 4

Conclusion

We have studied the $\eta_c N$ and the $J/\psi N$ interactions by the time-dependent HAL QCD method. The effective central potentials for the $\eta_c N$, the $J/\psi N$ with $J = 3/2$, and the $J/\psi N$ with $J = 1/2$ show that they are all attractive, and the attraction gets stronger in this order. The relatively small attraction of the $\eta_c N$ interaction than the $J/\psi N$ interactions can be explained by the chromoelectric dipole picture of the QCD van der Waals interaction. The scattering length a are: $a_{\eta_c N} = 0.246 \pm 0.026\,\mathrm{fm}$, $a_{J/\psi N J=1/2} = 0.656 \pm 0.071\,\mathrm{fm}$, and $a_{J/\psi N J=3/2} = 0.380 \pm 0.048\,\mathrm{fm}$, which are in rough agreement with previous lattice QCD calculations.

We have also determined the general form of the $J/\psi N$ potential at the lowest order of the derivative expansion. We have found there are four forces, *i.e.*, the central, the spin-spin, and two types of tensor forces. In the limit $m_c \to \infty$, the central force dominates the spin-dependent interactions, and have been simply neglected in most previous studies. We, for the first time, determined the four forces by lattice QCD first-principle calculations. The result shows that while the main contribution is from the central force, the spin-spin force gives sizeable correction to it. The tensor forces are both very small. The spin-spin force strengthen the attraction in the case of $J = 1/2$, while it weakens the attraction for $J = 3/2$.

Acknowledgements

I would like to thank my supervisor, Prof. Noriyoshi Ishii, for useful discusssion, as well as his gracious guidance throughout the 5 year experience at Osaka University. None of the results in this dissertation would have been achieved without his help. I am grateful for my collaborators, Prof. Makoto Oka, Prof. Yoichi Ikeda, and Dr. Keiko Murano for fruitful researches. Prof. Atsushi Hosaka and Prof. Kazuyuki Ogata have kindly given me a lot of insight to physics and useful comments on my research. They have also offered me support in a variety of educational affairs. I am very thankful to them. I have been very happy to spend time with all the (former) members of the RCNP theory group. Especially, I owe a lot to Ms. Mika Tambara and Ms. Sachiko Karasuyama for their support as a secretary of our group. Last but not least, I would like to thank my parents Yoichi and Yukie. They have not only economically supported me, but also assisted me to continue studies without stress or anxiety.

Appendix A

Spherical Harmonics with SO(3) symmetry

The $J/\psi N$ wave function has a Dirac spinor index $\alpha = 1, 2$ and a J/ψ spin index $\mu = 1, 2, 3$. By arranging α in rows and μ in columns, it can be written as a 2-by-3 matrix,

$$\psi^{(J,J_z,l,s)}(\boldsymbol{r}) = \{\psi_{\alpha\mu}(\boldsymbol{r})\} = \begin{pmatrix} \psi_{11}(\boldsymbol{r}) & \psi_{12}(\boldsymbol{r}) & \psi_{13}(\boldsymbol{r}) \\ \psi_{21}(\boldsymbol{r}) & \psi_{22}(\boldsymbol{r}) & \psi_{23}(\boldsymbol{r}) \end{pmatrix}, \tag{A.1}$$

supposing that this is an eigenstate with total angular momentum J, its z-component J_z, orbital angular momentum l, and total spin s. It is rewritten as

$$\psi^{(J,J_z,l,s)}(\boldsymbol{r}) = \langle \boldsymbol{r} \,|\, l, s; J, J_z \rangle \tag{A.2}$$

$$= \sum_{l_z=-l}^{+l} \sum_{s_z=-s}^{+s} \langle \boldsymbol{r} \,|\, l, s; l_z, s_z \rangle \langle l, s; l_z, s_z \,|\, l, s; J, J_z \rangle, \tag{A.3}$$

where we have used the identity

$$\mathbf{1} = \sum_{l_z=-l}^{+l} \sum_{s_z=-s}^{+s} |l, s; l_z, s_z\rangle \langle l, s; l_z, s_z| . \tag{A.4}$$

The factors $\langle l, s; l_z, s_z \,|\, l, s; J, J_z \rangle$ are the ClebschGordan coefficients. The wave function can be separated into a spatial part and an angular part as

$$\langle \boldsymbol{r} \,|\, l; l_z \rangle = u_l(r) \langle \hat{\boldsymbol{r}} \,|\, l; l_z \rangle \tag{A.5}$$

$$= u_l(r) Y_l^{l_z}(\hat{\boldsymbol{r}}), \tag{A.6}$$

where $\hat{\boldsymbol{r}} = \boldsymbol{r}/|\boldsymbol{r}|$ and the spherical harmonics are denoted as $Y_l^{l_z}(\hat{\boldsymbol{r}})$. We now define a spin harmonics $\mathcal{Y}_{J,J_z}^{(l,s)}(\hat{\boldsymbol{r}})$ as

$$\mathcal{Y}_{J,J_z}^{(l,s)}(\hat{\boldsymbol{r}}) = \sum_{l_z=-l}^{+l} \sum_{s_z=-s}^{+s} Y_l^{l_z}(\hat{\boldsymbol{r}}) \,|s; s_z\rangle \langle l, s; l_z, s_z \,|\, l, s; J, J_z \rangle, \tag{A.7}$$

so that Eq. (A.3) is rewritten as

$$\psi^{(J,J_z,l,s)}(\boldsymbol{r}) = u_l(r)\mathcal{Y}^{(l,s)}_{J,J_z}(\hat{\boldsymbol{r}}). \tag{A.8}$$

The total spin function $|s;s_z\rangle$ is a 2-by-3 matrix in the basis of α and μ. What we are left with is to derive the exact forms of the spin harmonics $\mathcal{Y}^{(l,s)}_{J,J_z}(\hat{\boldsymbol{r}})$.

The nucleon spin state are written as

$$|1/2;+1/2\rangle = \begin{pmatrix}1\\0\end{pmatrix}, \tag{A.9}$$

$$|1/2;-1/2\rangle = \begin{pmatrix}0\\1\end{pmatrix}, \tag{A.10}$$

whereas the J/ψ spin states are

$$|+1;1\rangle = -\frac{1}{\sqrt{2}}(1,i,0), \tag{A.11}$$

$$|-1;1\rangle = +\frac{1}{\sqrt{2}}(1,-i,0), \tag{A.12}$$

$$|0;1\rangle = (0,0,1). \tag{A.13}$$

From these matrices, the total spin functions are given as

$$|s,s_z\rangle = \sum_{m_1=\pm1/2}\sum_{m_2=0,\pm1}\langle 1/2,1;m_1,m_2\,|\,1/2,1;s,s_z\rangle\,|1/2,1;m_1,m_2\rangle. \tag{A.14}$$

Therefore we find that

$$|+1/2;1/2\rangle = \frac{1}{\sqrt{3}}\begin{pmatrix}0&0&-1\\-1&-i&0\end{pmatrix}, \tag{A.15}$$

$$|-1/2;1/2\rangle = \frac{1}{\sqrt{3}}\begin{pmatrix}-1&i&0\\0&0&1\end{pmatrix}, \tag{A.16}$$

$$|+3/2;3/2\rangle = \frac{1}{\sqrt{2}}\begin{pmatrix}-1&-i&0\\0&0&0\end{pmatrix}, \tag{A.17}$$

$$|+1/2;3/2\rangle = \frac{1}{\sqrt{6}}\begin{pmatrix}0&0&2\\-1&-i&0\end{pmatrix}, \tag{A.18}$$

$$|-1/2;3/2\rangle = \frac{1}{\sqrt{6}}\begin{pmatrix}1&-i&0\\0&0&2\end{pmatrix}, \tag{A.19}$$

$$|-3/2;3/2\rangle = \frac{1}{\sqrt{2}}\begin{pmatrix}0&0&0\\1&-i&0\end{pmatrix}. \tag{A.20}$$

The explicit forms of the spherical harmonics with $l = 0, 2$ are as follows.

$$Y_0^0(\hat{\boldsymbol{r}}) = \frac{1}{\sqrt{4\pi}}, \tag{A.21}$$

$$Y_2^{-2}(\hat{\boldsymbol{r}}) = \frac{1}{4}\sqrt{\frac{15}{2\pi}}\left(\hat{x}^2 - \hat{y}^2 - 2i\hat{x}\hat{y}\right), \tag{A.22}$$

$$Y_2^{-1}(\hat{\boldsymbol{r}}) = \frac{1}{2}\sqrt{\frac{15}{2\pi}}\left(\hat{x}\hat{z} - i\hat{y}\hat{z}\right), \tag{A.23}$$

$$Y_2^{0}(\hat{\boldsymbol{r}}) = \frac{1}{4}\sqrt{\frac{5}{\pi}}\left(-\hat{x}^2 - \hat{y}^2 + 2\hat{z}^2\right), \tag{A.24}$$

$$Y_2^{+1}(\hat{\boldsymbol{r}}) = -\frac{1}{2}\sqrt{\frac{15}{2\pi}}\left(\hat{x}\hat{z} + i\hat{y}\hat{z}\right), \tag{A.25}$$

$$Y_2^{+2}(\hat{\boldsymbol{r}}) = \frac{1}{4}\sqrt{\frac{15}{2\pi}}\left(\hat{x}^2 - \hat{y}^2 + 2i\hat{x}\hat{y}\right), \tag{A.26}$$

with

$$\hat{\boldsymbol{r}} = (\hat{x}, \hat{y}, \hat{z}). \tag{A.27}$$

Combining the above results, we find the spin harmonics as follows. (We drop obvious argument $\hat{\boldsymbol{r}}$ from $Y_l^{l_z}(\hat{\boldsymbol{r}})$.)

$$\mathcal{Y}^{(0,1/2)}_{1/2,+1/2} = \frac{1}{\sqrt{12\pi}}\begin{pmatrix} 0 & 0 & -1 \\ -1 & -i & 0 \end{pmatrix} \tag{A.28}$$

$$\mathcal{Y}^{(0,1/2)}_{1/2,-1/2} = \frac{1}{\sqrt{12\pi}}\begin{pmatrix} -1 & i & 0 \\ 0 & 0 & 1 \end{pmatrix} \tag{A.29}$$

$$\mathcal{Y}^{(2,3/2)}_{1/2,+1/2} = \frac{1}{\sqrt{60}}\begin{pmatrix} -\sqrt{3}Y_2^{+1} - \sqrt{3}Y_2^{-1} & i\sqrt{3}Y_2^{+1} + i\sqrt{3}Y_2^{-1} & 2\sqrt{2}Y_2^{0} \\ 2\sqrt{3}Y_2^{+2} - \sqrt{2}Y_2^{0} & -i2\sqrt{3}Y_2^{+2} - i\sqrt{2}Y_2^{0} & -2\sqrt{3}Y_2^{+1} \end{pmatrix} \tag{A.30}$$

$$\mathcal{Y}^{(2,3/2)}_{1/2,-1/2} = \frac{1}{\sqrt{60}}\begin{pmatrix} -\sqrt{2}Y_2^{0} + 2\sqrt{3}Y_2^{-2} & i\sqrt{2}Y_2^{0} + i2\sqrt{3}Y_2^{-2} & 2\sqrt{3}Y_2^{-1} \\ \sqrt{3}Y_2^{+1} - \sqrt{3}Y_2^{-1} & -i\sqrt{3}Y_2^{+1} - i\sqrt{3}Y_2^{-1} & -2\sqrt{2}Y_2^{0} \end{pmatrix} \tag{A.31}$$

$$\mathcal{Y}^{(0,3/2)}_{3/2,+3/2} = \frac{1}{\sqrt{8\pi}} \begin{pmatrix} -1 & -i & 0 \\ 0 & 0 & 0 \end{pmatrix} \tag{A.32}$$

$$\mathcal{Y}^{(0,3/2)}_{3/2,+1/2} = \frac{1}{\sqrt{24\pi}} \begin{pmatrix} 0 & 0 & 2 \\ -1 & -i & 0 \end{pmatrix} \tag{A.33}$$

$$\mathcal{Y}^{(0,3/2)}_{3/2,-1/2} = \frac{1}{\sqrt{24\pi}} \begin{pmatrix} 1 & -i & 0 \\ 0 & 0 & 2 \end{pmatrix} \tag{A.34}$$

$$\mathcal{Y}^{(0,3/2)}_{3/2,-3/2} = \frac{1}{\sqrt{8\pi}} \begin{pmatrix} 0 & 0 & 0 \\ 1 & -i & 0 \end{pmatrix} \tag{A.35}$$

$$\mathcal{Y}^{(2,1/2)}_{3/2,+3/2} = \frac{1}{\sqrt{15}} \begin{pmatrix} -2Y_2^{+2} & i2Y_2^{+2} & Y_2^{+1} \\ Y_2^{+1} & iY_2^{+1} & 2Y_2^{+2} \end{pmatrix} \tag{A.36}$$

$$\mathcal{Y}^{(2,1/2)}_{3/2,+1/2} = \frac{1}{\sqrt{15}} \begin{pmatrix} -\sqrt{3}Y_2^{+1} & i\sqrt{3}Y_2^{+1} & \sqrt{2}Y_2^{0} \\ \sqrt{2}Y_2^{0} & i\sqrt{2}Y_2^{0} & \sqrt{3}Y_2^{+1} \end{pmatrix} \tag{A.37}$$

$$\mathcal{Y}^{(2,1/2)}_{3/2,-1/2} = \frac{1}{\sqrt{15}} \begin{pmatrix} -\sqrt{2}Y_2^{0} & i\sqrt{2}Y_2^{0} & \sqrt{3}Y_2^{-1} \\ \sqrt{3}Y_2^{-1} & i\sqrt{3}Y_2^{-1} & \sqrt{2}Y_2^{0} \end{pmatrix} \tag{A.38}$$

$$\mathcal{Y}^{(2,1/2)}_{3/2,-3/2} = \frac{1}{\sqrt{15}} \begin{pmatrix} -Y_2^{-1} & iY_2^{-1} & 2Y_2^{-2} \\ 2Y_2^{-2} & i2Y_2^{-2} & Y_2^{-1} \end{pmatrix} \tag{A.39}$$

$$\mathcal{Y}^{(2,3/2)}_{3/2,+3/2} = \frac{1}{\sqrt{30}} \begin{pmatrix} \sqrt{2}Y_2^{+2} - \sqrt{3}Y_2^{0} & -i\sqrt{2}Y_2^{+2} - i\sqrt{3}Y_2^{0} & -2\sqrt{2}Y_2^{+1} \\ \sqrt{2}Y_2^{+1} & i\sqrt{2}Y_2^{+1} & 2\sqrt{2}Y_2^{+2} \end{pmatrix} \tag{A.40}$$

$$\mathcal{Y}^{(2,3/2)}_{3/2,+1/2} = \frac{1}{\sqrt{30}} \begin{pmatrix} -\sqrt{6}Y_2^{-1} & -i\sqrt{6}Y_2^{-1} & -2Y_2^{0} \\ \sqrt{6}Y_2^{+2} + Y_2^{0} & -i\sqrt{6}Y_2^{+2} + iY_2^{0} & 0 \end{pmatrix} \tag{A.41}$$

$$\mathcal{Y}^{(2,3/2)}_{3/2,-1/2} = \frac{1}{\sqrt{30}} \begin{pmatrix} -Y_2^{0} - \sqrt{6}Y_2^{-2} & iY_2^{0} - i\sqrt{6}Y_2^{-2} & 0 \\ \sqrt{6}Y_2^{+1} & -i\sqrt{6}Y_2^{+1} & -2Y_2^{0} \end{pmatrix} \tag{A.42}$$

$$\mathcal{Y}^{(2,3/2)}_{3/2,-3/2} = \frac{1}{\sqrt{30}} \begin{pmatrix} -\sqrt{2}Y_2^{-1} & i\sqrt{2}Y_2^{-1} & 2\sqrt{2}Y_2^{-2} \\ \sqrt{3}Y_2^{0} - \sqrt{2}Y_2^{-2} & -i\sqrt{3}Y_2^{0} - i\sqrt{2}Y_2^{-2} & -2\sqrt{2}Y_2^{-1} \end{pmatrix} \tag{A.43}$$

Bibliography

[1] See "http://pdg.lbl.gov/".

[2] S. Weinberg, Physica A **96**, no.1-2, 327 (1979).

[3] M. Taketani *et al.*, Prog. Theor. Phys. Suppl. **39**,1 (1967); **42**,1 (1968).

[4] R. Machleidt and I. Slaus, J. Phys. G **27**, R69 (2001).

[5] R. Machleidt, Phys. Rev. C **63**, 024001 (2001).

[6] V. G. J. Stoks, R. A. M. Klomp, C. P. F. Terheggen, and J. J. de Swart, Phys. Rev. C **49**, 2950 (1994).

[7] R. B. Wiringa, V. G. J. Stoks, and R. Schiavilla, Phys. Rev. C **51**, 38 (1995).

[8] S. Okubo, Phys. Lett. **5**, 165 (1963).

[9] G. Zweig, CERN Report No.8419/TH412 (1964).

[10] J. Iizuka, Prog. Theor. Phys. Suppl. **37**, 21 (1966).

[11] M. E. Luke, A. V. Manohar, and M. J. Savage, Phys. Lett. B **288**, 355 (1992).

[12] D. Kharzeev and H. Satz, Phys. Lett. B **334**, 155 (1994).

[13] S. J. Brodsky and G. A. Miller, Phys. Lett. B **412**, 125 (1997).

[14] S. J. Brodsky, I. Schmidt, and G. F. de Téramond, Phys. Rev. Lett. B **288**, 355 (1992).

[15] A. Yokota, E. Hiyama, and M. Oka, Prog. Theor. Exp. Phys. **2013**, 113D01 (2013).

[16] A. Yokota, E. Hiyama, and M. Oka, Few-Body Syst. **55**, 761 (2014).

[17] T. Appelquist, M. Dine, and I. Muzinich, Phys. Rev. D **17**, 2074 (1978).

[18] K. G. Wilson, Phys. Rev. **179**, 1499 (1969).

[19] K. G. Wilson and W. Zimmermann, Commun. Math. Phys. **24**, 87 (1972).

[20] W. Zimmermann, Ann. Phys. **77**, 570 (1973).

[21] E. Witten, Nucl. Phys. B **120**, 189 (1977).

[22] M. E. Peskin, Nucl. Phys. B **156**, 365 (1979).
G. Bhanot and M. E. Peskin, Nucl. Phys. B **156**, 391 (1979).

[23] K. Gottfried, Phys. Rev. Lett. **40**, 538 (1978).

[24] M. Voloshin, Nucl. Phys. B **154**, 447 (1979).

[25] M. I. Eides, V. Y. Petrov, and M. V. Polyakov, Phys. Rev. D **93**, 054039 (2016).

[26] M. I. Eides, V. Y. Petrov, and M. V. Polyakov, Eur. Phys. J. C **78**, no.1, 36 (2018).

[27] M. B. Voloshin, Prog. Part. Nucl. Phys. **61**, 455 (2008).

[28] T. Sugiura, Y. Ikeda, and N. Ishii, EPJ Web Conf. **175**, 05011 (2018).

[29] M. V. Polyakov and P. Schweitzer, Phys. Rev. D **98**, no.3, 034030 (2018).

[30] M. Lüscher, Math. Phys. **104**, 177 (1986).

[31] M. Lüscher, Math. Phys. **105**, 153 (1986).

[32] M. Lüscher, Nucl. Phys. B **354**, 531 (1991).

[33] N. Ishii, S. Aoki, and T. Hatsuda, Phys. Rev. Lett. **99**, 022001 (2007).

[34] S. Aoki, T. Hatsuda, and N. Ishii, Prog. Theor. Phys. **123**, no.1 (2010).

[35] S. Aoki *et al.* [HAL QCD Collaboration], Prog. Theor. Exp. Phys. **2012**, 01A105 (2012).

[36] T. Sugiura, N. Ishii, and M. Oka, Phys. Rev. D **95**, 074514 (2017).

[37] N. Ishii *et al.* [HAL QCD Collaboration], Phys. Lett. B **712**, 437 (2012).

[38] S. Aoki *et al.*, [PACS-CS Collaboration], Phys. Rev. D **79**, 034503 (2009).
See also "https://www.jldg.org/ildg-data/PACSCSconfig.html".

[39] S. Aoki, Y. Kuramashi, and S. i. Tominaga, Prog. Theor. Phys. **109**, 383 (2003).

[40] Y. Namekawa *et al.* [PACS-CS Collaboration], Phys. Rev. D **87**, 094512 (2013).

[41] K. Yokokawa, S. Sasaki, T. Hatsuda, and A. Hayashigaki, Phys. Rev. D **74**, 034504 (2006).

[42] T. Kawanai and S. Sasaki, PoS LATTICE **2010**, 156 (2010).

[43] T. Kawanai and S. Sasaki, Phys. Rev. D **82**, 091501 (2010).

[44] S. Okubo and R. E. Marshak, Ann. Phys. **4**, 166 (1958).